AG-336

3. CONVENTIONAL CORRECTIONS IN VENTILATED TEST SECTIONS

AUTHOR: ALEX KRYNYTZKY

	PAGE
3.1 BACKGROUND, ASSUMPTIONS, AND DEFINITIONS	3-5
3.2 WALL BOUNDARY CONDITIONS	3-7
3.2.1 IDEAL VENTILATED WALL BOUNDARY CONDITIONS	3-8
3.2.2 EXPERIMENTAL INVESTIGATIONS OF PERFORATED-WALL CHARACTERISTICS	3-10
3.2.3 EXPERIMENTAL INVESTIGATIONS OF SLOTTED-WALL CHARACTERISTICS	3-12
3.3 INTERFERENCE IN 2D TESTING	3-14
3.3.1 INTERFERENCE OF SMALL MODELS, UNIFORM WALLS	3-14
3.3.2 INTERFERENCE OF SMALL MODELS, NON-UNIFORM WALLS	3-16
3.4 INTERFERENCE IN 3D TESTING, CLASSICAL RESULTS	3-18
3.4.1 SLOTTED WALLS	3-19
3.4.2 POROUS WALLS	3-20
3.5 COMPUTATIONAL APPROACHES TO INTERFERENCE EVALUATION	3-22
3.5.1 POINT SINGULARITY MODEL REPRESENTATION	3-23
3.5.2 PANEL METHODS, HOMOGENEOUS VENTILATED WALLS	3-24
3.5.3 PANEL METHODS, FINITE-LENGTH AND DISCRETE SLOTS	3-27
3.6 CONCLUSION	3-41
NOMENCLATURE FOR CHAPTER 3	3-41
REFERENCES FOR CHAPTER 3	3-43

3. CONVENTIONAL CORRECTIONS IN VENTILATED TEST SECTIONS

Prior to the 1940s, closed-wall wind tunnels, and to a somewhat lesser extent, open-jet facilities, were the standard types of ground-based aerodynamic testing facilities. As described in Chapter 2, the fundamental characteristics of wall interference of small models in incompressible flow in these types of tunnel were established by the mid-1930s, e.g. Glauert [25]; Theodorsen, [62]). These analyses of lift and blockage interference in closed-wall and open-jet test sections predicted corrections of opposite sign. Reasoning that walls of some intermediate geometry would therefore minimise the interference, testing with walls having a mix of open and closed elements was undertaken.

Concurrent with these developments in testing methodology, the maturation of the applied aeronautical sciences (aerodynamics, structures, propulsion) was enabling flight speeds approaching the speed of sound. Investigation of aerodynamic characteristics of flight vehicles in closed-wall tunnels encounters serious difficulties in this speed range. Extremely small model sizes are required to avoid sonic choking of the flow around the model in a closed-wall test section. One-dimensional compressible flow relationships provide the limiting case of maximum model cross-sectional area for choked flow: for example, a model with an area blockage ratio of 0.01 permits a maximum upstream Mach number of only about 0.89. This problem is manifested even in linearised compressible flow, for which the Prandtl-Glauert compressibility transformation results in blockage interference velocities increasing like $1/\beta^3$ (Goethert [26]). The theoretical singularity at Mach = 1.0 (due to linearisation of the compressibility effect) is consistent with experimental difficulties experienced at high-subsonic test Mach numbers.

An unexpected consequence of testing with walls comprising both open and closed elements was a substantial increase in achievable upstream Mach number before the onset of sonic choking around the model. This discovery led to a new paradigm for wind tunnel testing at speeds where compressibility is no longer negligible: the ventilated wall. Two basic wall geometries have emerged as preferred ventilated wall types: slotted walls, comprising solid wall areas (slats) alternating with longitudinal slots, and perforated walls, which are characterised by a pattern of holes in an otherwise solid wall surface. Most commonly, the test section is surrounded by a single large open plenum chamber assumed to be at a constant static pressure that is usually used as the tunnel Mach number reference pressure, Figure 3.1. This plenum chamber may be vented at its downstream end to the test section diffuser through a variable-geometry re-entry flap system, or may be actively pumped by a plenum evacuation system (PES) which typically can remove up to several percent of the tunnel mass flow from the plenum, usually to be reinjected elsewhere into the tunnel circuit. Use of a PES is especially advantageous in the transonic speed range to maximise clear tunnel flow uniformity, to assist expansion of the upstream flow to supersonic test Mach numbers, and to help offset the adverse effects of wake blockage in the downstream part of the test section.

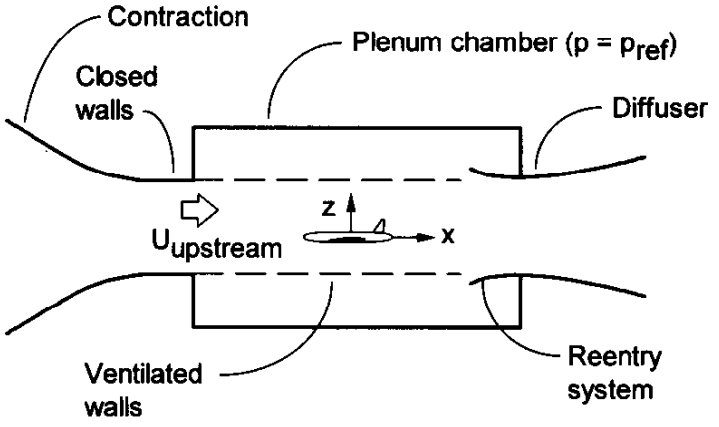

Figure 3.1 : Ventilated Wall Wind Tunnel, General Arrangement

Experience with slotted walls has led to their use primarily for subsonic testing. Perforated walls are preferred in the near-sonic and low-supersonic speed range, due to their ability to attenuate shock (and

expansion) wave reflections with the right choice of openness ratio (Estabrooks [17]; Jacocks [33]; Neiland [51]). Ventilated walls of one type or the other (or, in some cases, of a hybrid type), whose geometry remains fixed (or at most varies uniformly with Mach number) have been the mainstay of aerodynamic testing at Mach numbers from approximately 0.6 to 1.2 since their introduction in the 1940s and early 1950s (Goethert [27]).

With the maturation of aerodynamic testing technology, data accuracy needs have become more stringent (Steinle and Stanewsky [61]), with parallel accuracy requirements with regard to interference corrections. The continuing expansion of high Reynolds number testing (Goldhammer and Steinle [28]) has stimulated an increased appreciation of Reynolds number effects, which in turn has increased the pressure on model size in order to simulate flight Reynolds numbers more closely. Model size (relative to test section dimensions) thus continues to play a key role in interference calculations. Similarly, there is a continuing demand for more comprehensive predictions of flight characteristics, including increased emphasis on flight regimes where the effects of compressibility are strong (both on the flight characteristics themselves and on the wall interference as well). For subsonic flight vehicles whose design point is close to drag rise or beyond, this includes flight conditions at Mach numbers approaching 1.0, with substantial regions of supersonic flow, and possibly with large areas of separated flow. Supersonic flight vehicles require testing through their entire flight envelope, typically including Mach numbers as close to 1.0 as possible. Each of these factors increases the magnitude of the wall interference, consequently maintaining pressure on improving wall interference methods for ventilated wall tunnels.

Even though the theory of ventilated-wall wind tunnels is less soundly based than for closed-wall tunnels, conventional ventilated-wall tunnels offer several practical advantages: demonstrated small interference effects in subsonic flow (compared to closed-wall tunnels), the ability to operate at high-subsonic Mach number and through the sonic and low-supersonic speed range, and the operational simplicity of fixed-geometry ventilated walls. These advantages, coupled with both a substantial capital investment in existing test facilities and continuing competitive pressure to improve wind tunnel data accuracy, provide the motivation to understand ventilated wall behaviour.

Perhaps the greatest difficulty in the application of the methodology and results of ventilated-wall interference theory is the approximate nature of the ideal ventilated-wall boundary conditions and the unknown relationship between physical wall geometry and wall crossflow parameters. This weakness has motivated investigations of crossflow characteristics of particular wall geometries, the use of measured boundary conditions to determine wall characteristics (e.g., Mokry et al. [47]), development of alternate wall crossflow models, and finally, the direct use of measurements near the wall as boundary conditions in the computation of interference (see Chapter 4). The application of boundary measurement techniques for interference estimation of ventilated walls appears to be a viable approach, particularly for perforated walls (e.g., in 2D, Mokry and Ohman [48]; in 3D, Mokry, Digney, and Poole [50], Beutner, Celik, and Roberts [9], and even for slotted walls (Freestone and Mohan [22]). Nonetheless, because of the additional instrumentation, measurement, and computational requirements of such methods, testing with passive, nonadaptive, ventilated walls and the use of classically based corrections predominates in practice, especially for 3D tunnels.

The impact of improvements in high-speed computing cannot be overemphasised. The CFD codes and techniques developed over the past three decades for analysis of flight vehicles in an unconstrained flow are now being applied to the analysis of models within wind tunnels. More complex and larger test configurations, asymmetric installations in the test section, general tunnel cross sections, and a variety of

wall boundary conditions can now readily be analysed. The influences of finite test section length and model supports can also be evaluated.

3.1 BACKGROUND, ASSUMPTIONS, AND DEFINITIONS

"Conventional" wall corrections are taken to be those that apply to tunnel flows where the influence of the walls is approximated as an incremental flow field in the vicinity of the model that is calculable using linearised potential flow theory, and where the walls are basically of fixed geometry with known crossflow characteristics. Thus it is assumed that the flow around the model in the wind tunnel is governed by Equation 2.3, subject to the limitations described in Section 2.1. The potential at any point in the tunnel is expressed as the superposition of the separate potentials representing a uniform onset free stream, the model, and the walls (see Chapter 2):

$$\Phi(x,y,z) = -U_\infty x + \varphi_m(x,y,z) + \varphi_w(x,y,z) \tag{3.1}$$

Compressibility is taken into account through the Prandtl-Glauert compressibility factor β. The interference flow field is due to simply the wall potential. The test section is usually taken to be of constant section throughout its length, with flow through the walls satisfying a boundary condition relating the crossflow velocity and the pressure difference across the walls, Figure 3.2. For analytic solutions the tunnel is typically taken to be doubly infinite in length. When computational approaches such as panel methods are used, tunnel length is necessarily finite, but (usually) long. Model flows with substantial embedded supersonic regions, at high lift coefficients so that wake position or separated wake effects become important, and in the transonic, near-sonic, and low-supersonic speed regimes are beyond the scope of this chapter.

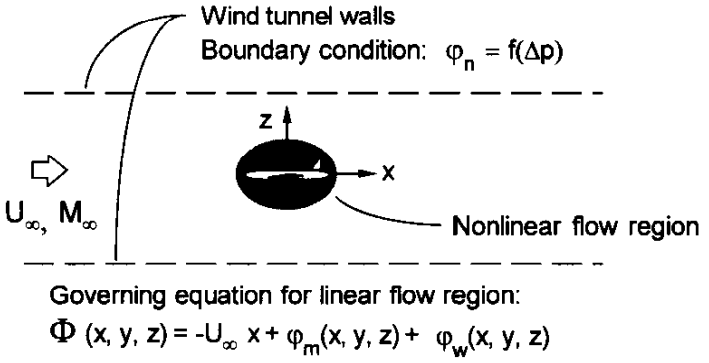

Figure 3.2 : Potential Flow in an Ideal Wind Tunnel With Ventilated Walls

"Conventional" ventilated walls are taken to be either longitudinally slotted walls, perforated walls, or a combination of these two wall types, whose behaviour is described locally by a simple pressure-crossflow relationship (see Sec. 3.2.1) and whose geometry remains fixed over a given range of test conditions. It is assumed that these walls are vented to a single large plenum chamber, whose pressure is constant and is taken to be the reference static pressure for the calculation of the onset Mach number in the tunnel. Note that for a plenum of finite longitudinal extent, the Mach number far upstream does not necessarily correspond to this plenum reference Mach number.

AGARDograph 109 [24]) provides a comprehensive review of a wide variety of wall configurations and their interference. In general, the interference of ventilated walls had not been investigated to the same level of detail as corresponding closed-wall configurations. Admittedly, contributing factors to this state of affairs include the additional wall parameters (which increase the number of cases of interest), the additional analytic and computational complexities associated with ventilated-wall boundary conditions, and the recognised approximate nature of these boundary conditions. In particular, only limited or no

interference information is given for rectangular tunnels with all four walls slotted or perforated (see Table 6.I of AGARDograph 109). Interference calculations for some of these cases have since been published (Pindzola and Lo [53]; Lo and Oliver [43]; Keller and Wright [38]).

The wall interference corrections in AGARDograph 109 for steady flows are discussed in terms of interference velocity components: longitudinal (or streamwise, u_i) and cross-stream (typically upwash, w_i). Because of their one-to-one correspondence to simple representations of model volume and lift for a model at the centre of a tunnel with uniform walls, these interferences are commonly referred to as blockage and lift interference, respectively. The separate interference velocity components are assumed to be independent and superposable. Independence can be obtained by suitable symmetry restrictions: a small model located at the centre of a tunnel of symmetric cross section and having uniform walls. Cross-coupling of interference velocity components and model characteristics (blockage interference due to lift, for example) will occur for models asymmetrically located relative to the walls and for non-linear wall crossflow characteristics. Non-linear wall ventilation can be the result of actual geometric differences among the walls, but is usually attributed to the action of viscosity at the walls. Superposition is valid provided the magnitudes of the corrections remain small and the Mach number is not too close to 1.0.

Interference corrections for ventilated walls are further classified in AGARDograph 109 according to wall type and test section cross section. The wall type refers to the boundary condition to be satisfied at the wall, mainly: closed-wall, open-jet, ideal slotted, or ideal porous, though there is some discussion of the hybrid slotted wall (slots with crossflow resistance). The test sections considered are the 2D tunnel (planar flow), circular (or by co-ordinate transformation, elliptical), rectangular and, less comprehensively, octagonal (or rectangular with corner fillets). Most of the results given are for walls whose geometry does not vary streamwise and that extend far upstream and downstream of the model.

As suggested in Chapter 2, the interference results for small models in 2D and rectangular test sections are considered suitably representative of many interference situations encountered in practice (the major exclusions include sidewall interference in 2D testing, "large" models, and models "too close" to the walls). Rectangular sections with corner fillets or elliptical cross sections may be approximated by rectangular tunnels of equal cross-sectional area and equivalent aspect ratio (width to height ratio). This approximation is supported by the close correspondence of interference characteristics of square and circular ventilated test sections.

For a small model, a subsonic onset Mach number not too close to 1.0, and for attached flow over the model, the variation of the interference flow field is negligible throughout the model volume, so that primary corrections to the freestream magnitude and direction are adequate. As discussed in Chapter 4, small embedded regions of supersonic flow around the model may be permitted. For larger models, or for more accurate correction, consideration of linear streamwise variations of interference velocities may be necessary. These result in buoyancy corrections to model drag and additional corrections to angle of attack (or lift) and pitching moment due to streamwise curvature. Non-linear streamwise or significant spanwise variation of interference may be addressed using the methods for residual interference corrections outlined in Section 1.3. The flow field around very large models may ultimately not be easily correctable to equivalent freestream conditions.

The interference flow field is commonly described in nondimensional terms as defined in Equations 2.6 and 2.8 for streamwise and cross-stream (upwash) interference velocity perturbations:

$$\varepsilon = \frac{u_i}{U_\infty} \tag{3.2}$$

$$\delta = \frac{w_i}{U_\infty}\frac{C}{SC_L} \tag{3.3}$$

Solid blockage interference for small models in ventilated-wall tunnels is conveniently expressed in terms of the blockage parameter Ω_S, the ratio of solid blockage in the ventilated test section to that in a closed-wall test section of the same cross section:

$$\Omega_S = \frac{\varepsilon_{ventilated}}{\varepsilon_{closed}} \tag{3.4}$$

Thus, Ω_S=1 for a closed-wall test section. Some basic classical results for ε_{closed} for small models in 2D and rectangular test sections are given in Chapter 2.

The streamwise gradient of ε, $\partial\varepsilon/\partial x$, results in a pressure force on the model (buoyancy drag), whose magnitude is proportional to the effective volume of the model (for small models in linear gradients). The streamwise gradient of upwash, or flow curvature, characterised by

$$\delta_1 = \frac{\partial\delta}{\partial(\frac{x}{\beta L})} \tag{3.5}$$

results in additional angle-of-attack and pitching moment corrections for even small models.

For models of large size, applying only primary corrections to the free stream is at best approximate. Residual corrections may be adequate for many cases but large variations of blockage and/or upwash interference over the region occupied by the model may ultimately not be correctable. That is, there is no equivalent unconstrained flow (with a uniform onset velocity) for the model geometry being tested. This situation is particularly acute in transonic flow fields because of their extreme sensitivity to small variations in onset flow conditions. The adequacy of corrections can be tested by careful comparison of computed model aerodynamic characteristics from in-tunnel and unconstrained-stream solutions (at flight conditions that include primary interference corrections). Such a test requires a higher degree of sophistication of model representation than for the calculation of simple linearised corrections. Paneling or gridding requirements for this type of analysis are the same as for typical high-resolution free-air analyses.

3.2 WALL BOUNDARY CONDITIONS

The wall boundary condition distinguishes ventilated walls from closed-wall or free-jet boundaries. A useful simplification of the actual wall boundary condition is to treat the walls as homogeneous, wherein the open- and closed-wall areas are not represented separately, but as an equivalent permeable surface (Davis and Moore [14]; Goethert [27]). The normal velocity through the walls thus is a local average, varying smoothly and in a continuous manner as a function of the (similarly spatially averaged) pressure distribution on the walls. Walls with perforations are thus idealised as permeable porous surfaces with infinitesimally small holes. Slotted tunnels are idealised as having an infinite number of very small slots distributed around the tunnel boundaries.

The validity of the assumption of homogeneous walls depends on the length scale of the wall openness and the Mach number. It is expected that the effect of wall "graininess" will be felt out into the tunnel stream a distance on the order of L/β, where L is the length scale associated with the wall openings. As long as L/β is small compared to the tunnel dimension (or more directly, to the distance from the wall to the closest model part, such as a wing tip), the interference felt by the model will be the same for homogeneous walls as for discretely ventilated walls having equivalent crossflow properties. There are often two distinct geometric length scales associated with a given ventilated wall: the typical size of the discrete openings and their spacing. A third length scale may also be involved: the wall boundary layer thickness, whose properties have been found to influence the wall crossflow characteristics.

For perforated walls, the openness length scales are the hole diameter and spacing. For slotted walls, they are the slot width and circumferential slot spacing. Consideration of typical perforated wall arrangements suggests that treating perforated walls as homogeneous (for wall interference purposes) is a valid assumption given the typical small scale of perforations. Slotted-wall openness length scales, on the other hand, are often at least an order of magnitude larger. For some tunnels, the slot spacing approaches a substantial fraction of a test section dimension. The assumption of homogeneous walls is more tenuous in this case, especially for models whose components are on the order of an openness length from a wall surface (e.g., wing tips of large-span models, body tail or nose for long models at high angles of attack).

For cases where the walls cannot be treated as homogeneous, the alternating open- and closed-wall areas (slots and slats) can be modelled separately, for example, by an appropriate mix of closed-wall and open-jet boundary conditions. In such situations, simplicity and computational efficiency are sacrificed for higher fidelity of the simulation.

Measured boundary condition methods with ventilated walls may be strongly influenced by wall inhomogeneities (closed and open elements). The resulting local flow gradients are not representative of the far-field homogeneous boundary condition. Correction methods for individual measurements, alternate measurement strategies, or explicit computational modelling of wall elements may be required.

3.2.1 IDEAL VENTILATED WALL BOUNDARY CONDITIONS

The boundary conditions of ventilated walls are motivated by physical considerations (see, for example, Davis and Moore [14]; Baldwin et al. [3]; Goethert [27]). The so-called ideal porous wall boundary condition can be derived by consideration of porous walls as a lattice of lifting elements. The pressure difference across the wall is then proportional to the flow inclination (θ) at the wall,

$$C_{p_{wall}} = \frac{p_{wall} - p_{plenum}}{q_\infty} = \frac{2}{R}\frac{v_{normal}}{U_\infty} = \frac{2}{R}\theta \tag{3.6}$$

In linearised perturbation form, with the plenum pressure taken to be the same as the pressure far upstream,

$$\varphi_n = -R\varphi_x \tag{3.7}$$

where R is an experimentally determined constant of proportionality. Note that the limits R=0 and $R\to\infty$ correspond to the standard closed-wall and free-jet boundary conditions, respectively. It is convenient to define an alternate perforated wall parameter,

$$Q = \frac{1}{\left(1 + \beta/R\right)} \tag{3.8}$$

so that Q=0 corresponds to a closed wall, and Q=1 to a free jet.

The ideal homogeneous slotted-wall boundary condition is developed by consideration of the balance of pressure difference across the slots and streamwise flow curvature in the vicinity of the slots,

$$\varphi_x + K\varphi_{xn} + \frac{\varphi_n}{R} = 0 \tag{3.9}$$

where the third term represents a viscous pressure drop across the slot and K, the slot parameter, is related to slot geometry, including the approximate effect of slot depth (t/a), according to

$$K = d\left[\frac{1}{\pi}\log_e\left(\operatorname{cosec}\frac{\pi a}{2d}\right) + \frac{t}{a}\right] \tag{3.10}$$

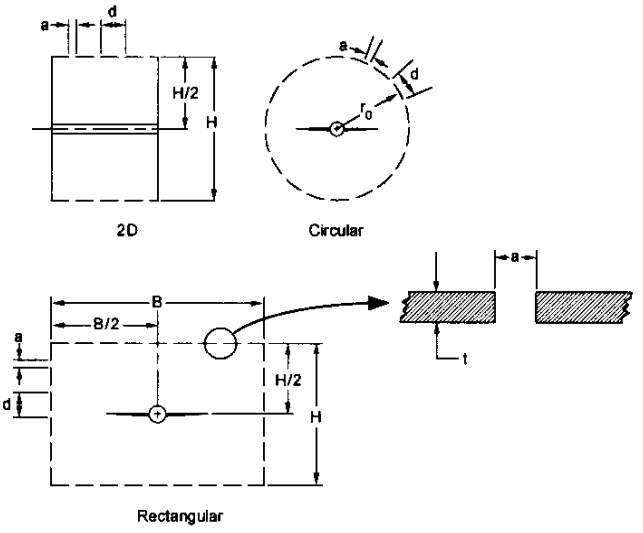

Figure 3.3 : Slotted Tunnel Geometry

Slotted-wall geometry definitions are summarised in Figure 3.3. For an ideal inviscid slotted wall (i.e., $R\to\infty$), closed-wall and free-jet boundary conditions correspond to $K\to\infty$ and K=0, respectively. As for the ideal porous wall, a convenient alternate slot parameter is defined,

$$P = \frac{1}{1+F} \tag{3.11}$$

where F is proportional to K according to

$F = 2\,K\,/\,H$ for a 2D test section.
$F = K\,/\,r_0$ for a circular test section.
$F = K\,/\,H$ for a rectangular test section.

P=0 and P=1 correspond to closed-wall and free jet boundary conditions respectively.

The boundary conditions for walls with discrete slots comprise

$\varphi_n = 0$ on the slats (i.e., the closed-wall segments between slots).
$\varphi_x + \varphi_n\,/\,R = 0$ for slots with crossflow resistance.
$\varphi_x = 0$ for open slots.

The ideal ventilated-wall boundary conditions may be viewed as first-order approximations to ventilated-wall crossflow characteristics. These simple analytic expressions are intended to capture the dominant flow physics at the wall, as perceived at some distance from the wall (i.e., at the model location). Improvements in ventilated wall modelling have focused on more accurate descriptions of the flow near the wall, including:

1) Effect of boundary layer thickness on the wall crossflow characteristics.
2) Non-linear pressure-drop terms (e.g. proportional to square of crossflow velocity).
3) Entry of stagnant plenum air into the test section.

3.2.2 Experimental Investigations of Perforated-Wall Characteristics

Many investigations, both theoretical and experimental, have been undertaken to capture the behaviour of various perforated-wall geometries. Perforated walls are taken to be any wall with a pattern of small openings, usually round holes drilled either normal to the wall surface or at a fixed angle to the normal. Variable porosity features have been implemented in several facilities using a sliding backing plate. Figure 3.4 illustrates some typical perforated wall configurations. Slanted hole walls were developed to offset the observed lower resistance to inflow compared to outflow. A large number of configuration variations have been tested, including splitter plates and screens in the openings to attenuate discrete noise tone production, various hole patterns, openness ratios, and hole angles.

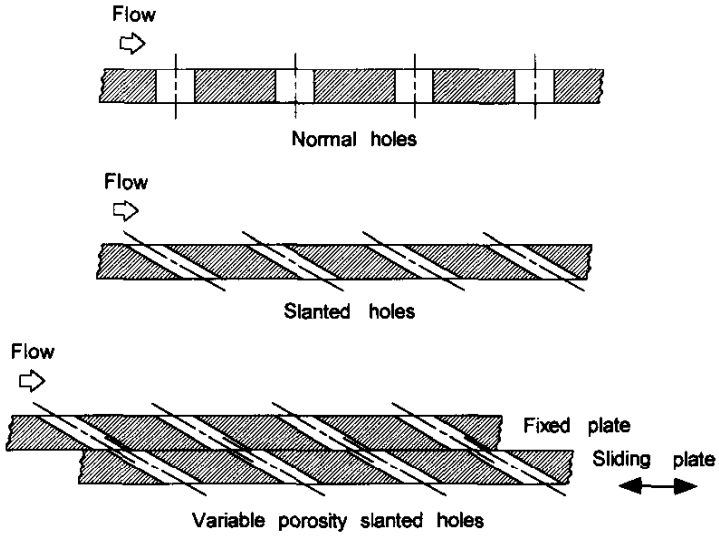

Figure 3.4 Perforated Wall Configurations

Two general approaches for the determination of a pressure-crossflow relationship may be distinguished. The first relies on explicit measurement (or calculation) of both pressure difference and crossflow at the wall. Methods for determination of the velocity normal to the wall include direct velocity measurements near the wall, massflow measurement through a portion of wall vented to an otherwise sealed and pumped plenum, and a hybrid theoretical-experimental method for the calculation of crossflow at the wall. Pressure differences across the wall may be applied either by a model in the test section, or by active plenum pumping with a "clear" test section. The second approach uses measured wall pressure differences, but avoids the direct measurement or calculation of crossflow velocity at the wall. The necessary information for determining wall characteristics may come from wall pressure correlations (test-theory), from tests of a model in several facilities, or tests of geometrically similar models in the same facility. The starting point for the latter two approaches is a set of interference-free data (e.g., small model in a very large tunnel) and a methodology for extracting lift and blockage interference from comparisons of model data.

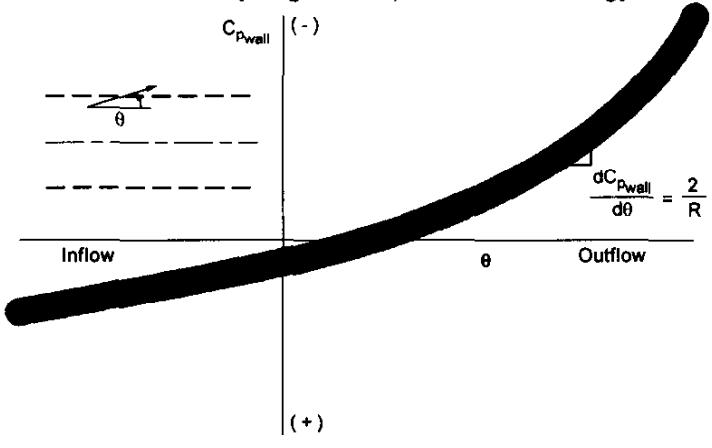

Figure 3.5 Non-linear Porous-Wall Crossflow Characteristics

Some of the deviations from linear crossflow behaviour that have been experimentally observed are illustrated in Figure 3.5. These include non-zero crossflow at zero pressure difference across the walls, different initial slopes for inflow and outflow, and non-linear behaviour as crossflow velocities increase. These behaviours are attributed to the effect of the wall boundary layer. Several experimental investigations have therefore focused on

correlations of these additional parameters with wall boundary layer thickness.

A first step toward characterising the interference of walls with non-linear wall resistance would be simply to model different wall resistance for inflow and outflow. Mokry, Peake, and Bowker [47] allow opposing perforated walls (20.5 percent openness normal holes in 2D testing) to have different resistance, based on the observation that for an airfoil with lift, measured wall pressures on opposite walls are of opposite sign relative to the plenum, so that the floor would experience primarily outflow, and the ceiling, inflow to the test section. This approach results in much better correspondence of predicted wall pressures to measurements than use of the same resistance for both floor and ceiling. For cases shown, the ceiling R value (inflow) is about three times larger than the floor R value (outflow). Chan [11] establishes a correlation of wall crossflow characteristics for inflow to the test section that depends explicitly on the wall boundary layer displacement thickness. Two correlations are given: a quadratic relationship of wall mass flux as a function of C_p δ^*/d for $\delta^*/d \leq 0.25$ and a linear relationship between wall mass flux and wall C_p for $\delta^*/d > 0.25$.

Jacocks [34] presents wall crossflow characteristics for slanted-hole perforated walls (holes drilled at 60 deg from the normal), including variable porosity configurations and the effects of screens and splitter plates for edge-tone noise suppression. Test Mach numbers ranged from 0.5 to 0.85 with limited results at 0.9 and 1.2. A combined experimental-theoretical approach is used to calculate the crossflow at the wall, thus sidestepping the direct measurement of mass flux through the wall (limited crossflow measurements were made in order to validate the method). Some configurations tested clearly exhibit differential resistance of inflow and outflow. Decreased wall resistance resulted from increasing porosity and also from increased boundary layer thickness. The value of R increased by factors of 2 to 3 (depending on wall configuration) for δ^*/d varying between about 0.1 to almost 1.0. It is suggested that the results of Mokry et al. [47] are the result of a thicker boundary on the inflow wall. The addition of screens improved crossflow linearity. It is concluded that most, but not all, perforated walls can be assumed linear for purposes of calculating subsonic wall interference. However, each wall of a given wind tunnel may require a different characterisation to capture differences in mean wall boundary-layer thicknesses.

Matyk and Kobayashi [44] report direct measurements of wall crossflow as a function of pressure across the wall for wall samples with baffled slots representing the wall configurations of the Ames 2-ft by 2-ft and 11-ft by 11-ft transonic wind tunnels. Data for only outflow were acquired over a range of $\Delta p/q_\infty$ from 0 to 0.5 and higher. Significant non-linear behaviour was observed for wall normal massflow ratios above approximately 0.04. Wall characteristics were consistent across the tested Mach number range ($0.5 < M < 1.2$).

Ivanov [32] reports very good linear crossflow behaviour of wall samples with normal holes in a wind tunnel with a relatively thick wall boundary layer (displacement thickness to hole diameter ratios greater than 1). Characteristic slopes differing by more than a factor of 2 were determined for inflow and outflow with no discernible trend with Mach number ($0.4 < M < 0.98$).

Vayssaire [67] summarises values of R deduced from experiments comparing model measurements with different walls. This method relies on model data from a closed-wall tunnel for which corrections are nominally known. For example, mapping of a model characteristic (such as shock position) from ventilated wall tests to corrected closed-wall data provides the ventilated-wall blockage correction, from which an average effective wall characteristic can be inferred using theoretical curves. Other corrections are then calculated using this inferred wall resistance. Pounds and Walker [54] similarly deduce global R

values for variable-porosity walls from measured lift curves of a semispan wing-body model using data from a large tunnel as the interference-free baseline.

Starr [58] used pressure distributions on a cone-cylinder model in a Ludwieg tube at Mach numbers between 0.95 and 1.2 to assess effective wall porosity sensitivity (for slanted holes at 60 deg from the normal) to wall boundary layer changes. For δ^*/d varying from about 0.13 to 0.28 the equivalent wall porosity change was found to be about 1 percent.

Crites and Rueger [13] provide a wall crossflow correlation for a set of five perforated wall samples of various geometries. Their results are similar to Chan [11] in that the quadratic dependence of crossflow on wall pressure is much greater for inflow to the test section than for outflow.

In summary, R values estimated for different tunnels exhibit a large degree of variability, even for similar nominal openness. Wall boundary layer thickness, especially in regions of inflow to the test section, appears to play a dominant role in wall resistance. The observed linearity of the wall pressure-crossflow relationship under many conditions leaves open the possibility of adequate wall corrections using locally linear approximations. However, allowance for variation of the wall resistance factor with inflow and outflow or with wall boundary layer thickness is likely required for high-quality wall interference predictions. The inclusion of a quadratic crossflow term is recommended by some investigators, though simple linear characterisations appear to work well for small wall crossflow. Because of the dependence of wall performance on wall boundary layer (which may in turn depend on plenum suction), it is recommended that wall resistance values or curves (R or $dCp/d\theta$ vs. wall openness) be determined for each facility under typical operating conditions according to desired accuracy requirements.

3.2.3 Experimental Investigations of Slotted-Wall Characteristics

The investigation of flow through open slots has advanced on several fronts. The effect of wall thickness has been explored using inviscid slot flow models. Experimental measurements aimed at establishing the slotted-wall boundary condition have successfully documented the richness of flow phenomena through slots and have been instrumental in guiding the development of slot models.

The effect of wall thickness on slot parameter K has been investigated by Chen and Mears [12] for ideal slots without crossflow resistance using a potential-flow doublet-rod wall model. Barnwell [4], as well as correcting an error in the preceding analysis, generalises the flat-slat boundary condition to a slot with sidewalls or separation in the plenum. He concludes that for the sidewall case (i.e., deep slots of constant width),

$$K_{sidewalls} = \frac{1}{\pi}\log_e \frac{d}{2a} \tag{3.12}$$

For the case of separation on the plenum side,

$$K_{separated} = \frac{1}{\pi}\log_e\left[\frac{2+\pi}{4\pi}\frac{d}{a}\right] \tag{3.13}$$

For small a/d, Equations 3.10, 3.12, and 3.13 provide only slightly different values of K. A greater cause for concern involves the experimental determination of K. Continuing research at NASA Langley aimed at validating a slot-flow model (Barnwell [5], Everhart and Barnwell [18]) included evaluation of K from measurements near a slotted wall in a 2D tunnel. Figure 3.6, from Everhart [19]), summarises some of

these results. Everhart's results for a four-slot wall configuration compare favourably with other published experimental values, which all deviate significantly from the inviscid slotted-wall theoretical predictions.

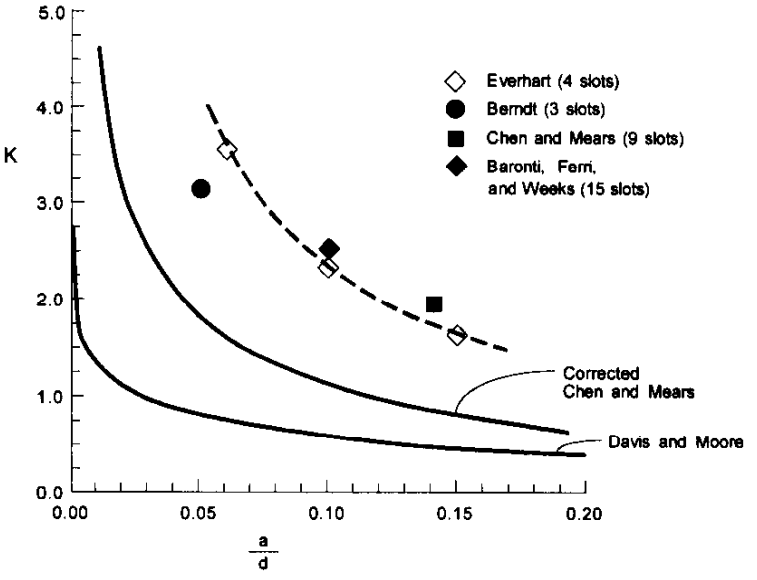

Figure 3.6 Experimental Values of Ideal Slot Coefficient, M = 0.7 (after Everhart [18])

Experimental confirmation of pressure drop proportional to crossflow velocity in the slotted-wall boundary conditions, as suggested by Baldwin et al. [3], is given by Goethert [27] for a single open slot, with a quadratic dependence (for outflow) becoming apparent above a wall pressure coefficient of about 0.04. Everhart [19] confirms a quadratic pressure-crossflow relationship for large crossflows in the absence of flow curvature. Nevertheless, it is concluded that the ideal form of the slotted-wall boundary condition (Eq. 3.9 with $R \to \infty$) describes the wall pressure drop upstream of the maximum model thickness if a reference pressure zero-shift is included. Downstream of this point wall pressures are only qualitatively predicted.

The above investigations have benefited from parallel theoretical and experimental developments (Berndt and Sorensen [8]; Berndt [6]; Nyberg [52]; Berndt [7]), which have resulted in a slot-flow model motivated by observed slot-flow physics. The boundary between high-velocity air originating in the test section and quiescent air from the plenum is tracked, and empirical coefficients are used to account for flow separation at the slot edges and for viscous flow within the slot, Figure 3.7. This method has shown good correlation (using the non-linear perturbation potential flow equation) with measured wall pressures at Mach numbers up to 0.98 and has been used to design the contoured slots for the FFA T1500 Transonic Wind Tunnel (Karlsson and Sedin [36]; Sedin and Sorensen [56]; Agrell, Pettersson, and Sedin [1]; Agrell [2]). Firmin and Cook [21] provide independent experimental confirmation (from pitot-static probe measurements and oil flow visualisation near the slots) of the penetration of low-energy plenum air into a slotted test section downstream of an airfoil model. This penetration is cited as a serious obstacle for determination of an equivalent homogeneous

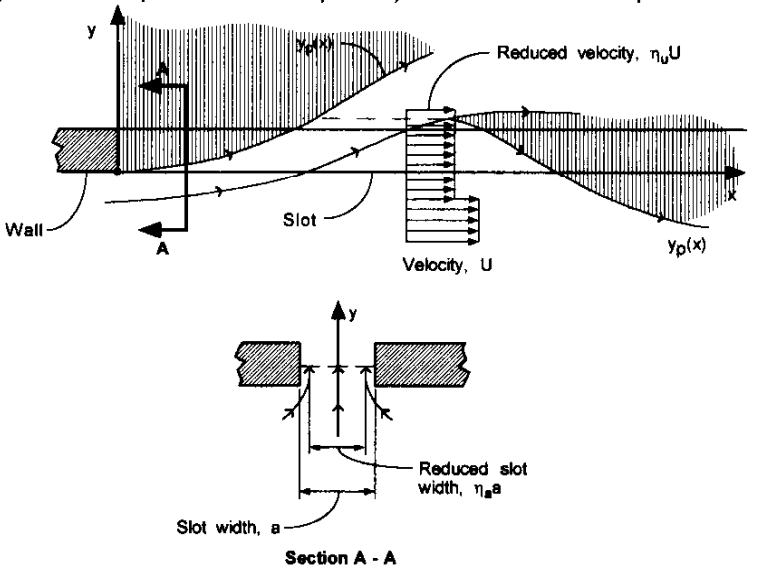

Figure 3.7 : Slot Flow Model (after Sedin and Sorensen [54])

boundary condition for slotted walls. It is suggested that porous walls behave similarly with regard to low-energy re-entry flow, but wall homogeneity would not be an issue due to the smaller length scales of the wall ventilation.

In addition to the work reported above, other investigators have reported the results of flowfield measurements in the vicinity of slots. Wu, Collins, and Bhat [68] document the 3D character of the flow near a single baffled slot with varying suction through the slot. They measured a vortex-like secondary flow in the crossflow plane whose effect extended beyond the edge of the boundary layer at low suction rate. Suction was found to have a large effect on boundary layer displacement thickness on the slat. A non-linear relationship between crossflow velocity at the slot and at the edge of the boundary layer (the equivalent inviscid crossflow) was measured. Everhart, Igoe, and Flechner [20] provide a database of flowfield measurements near and within an open slot, including the effects of plenum suction and the presence of a model (NACA 0012-64 2D airfoil). In the course of the development of a "two-variable" boundary interference approach for slotted walls, Freestone and Mohan [22] show good agreement between measured and predicted slot flows in a low-speed test of a large 2D airfoil. Slot flows are measured using a traversing flow-angle probe; predictions are from the slot-flow model of Berndt and Sorensen [8] with the addition of a linear resistance term for flow into the test section.

3.3 INTERFERENCE IN 2D TESTING

Some of the principal results given in AGARDograph 109 and Pindzola and Lo [53] for small models are repeated here as benchmarks. These results were calculated using a Fourier transform method.

Engineering Sciences Data [15] has published comprehensive summary carpet plots of lift and blockage interference and gradient factors for 2D point singularities in ideal porous and slotted test sections.

3.3.1 INTERFERENCE OF SMALL MODELS, UNIFORM WALLS

Interference parameters for a small model in the centre of a 2D test section with (homogeneous) slotted and porous walls are shown in Figure 3.8 as functions of slotted wall parameter P, and porous wall parameter Q, respectively. The model is represented as the superposition of a point vortex whose strength is proportional to lift, and by a point source doublet whose strength is proportional to the model effective cross-sectional area. It is recalled (Eq. 2.45, Sec. 2.2.1.1) that the blockage of a small model in a 2D closed-wall test section is given by

$$\varepsilon_{closed} = \frac{\pi}{6}\frac{A}{\beta^3 H^2} \tag{3.14}$$

where A is the effective cross-sectional area of the model and H is the height of the test section.

Although the closed-wall and open-jet limits of P and Q (0 and 1, respectively) are the same for these two types of walls, the interference characteristics at intermediate values of P and Q are fundamentally distinct (except when consideration is given to slots with crossflow resistance). From Figure 3.8 it can be seen that it is not possible to obtain zero blockage and zero upwash interference simultaneously with any uniform porous wall or uniform inviscid slot geometry.

The longitudinal distribution of blockage interference midway between the walls (for a model likewise located) is shown in Figure 3.9. For ideal slotted walls with no viscous pressure-drop term (Q=0), the

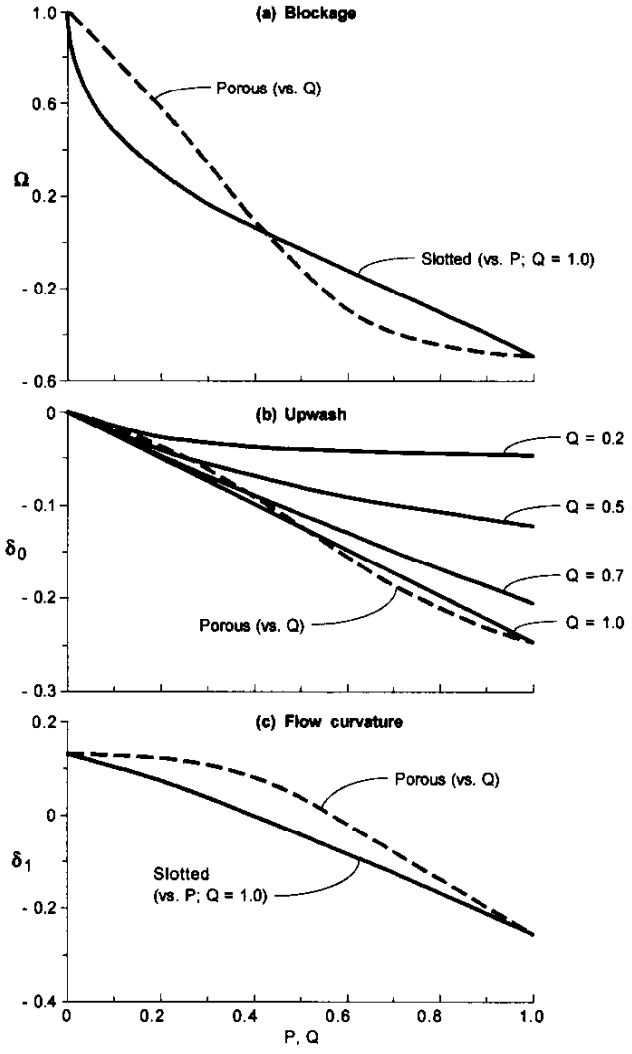

Figure 3.8 2D Interference in Ideal Slotted and Porous Tunnels

interference velocity along the tunnel centreline is symmetric fore and aft of the model. Consequently, there is no interference buoyancy force on the model. In contrast, porous walls (except for the limiting cases of closed and open jets) exhibit a longitudinal interference gradient, producing a buoyancy force on the model. The gradient is very nearly a maximum for the value of porosity for zero blockage interference (Pindzola and Lo [53], Figure 3.5). Similar interference distributions can be expected for slots with non-zero Q.

The longitudinal variation of upwash interference is shown in Figure 3.10 for ideal slotted and porous walls (Pindzola and Lo [53]). Zero upwash at the model location is obtained for closed walls only. Zero upwash gradient is obtained for intermediate values of P and Q (for slotted and porous walls, respectively), but the upwash is non-zero for these cases.

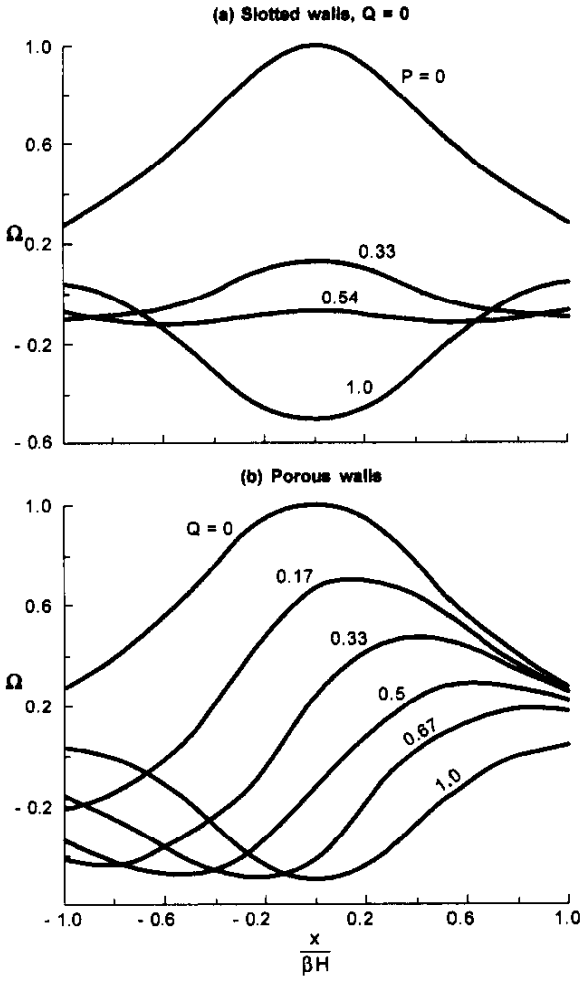

Figure 3.9 Longitudinal Variation of Blockage Interference in 2D Slotted and Porous Tunnels

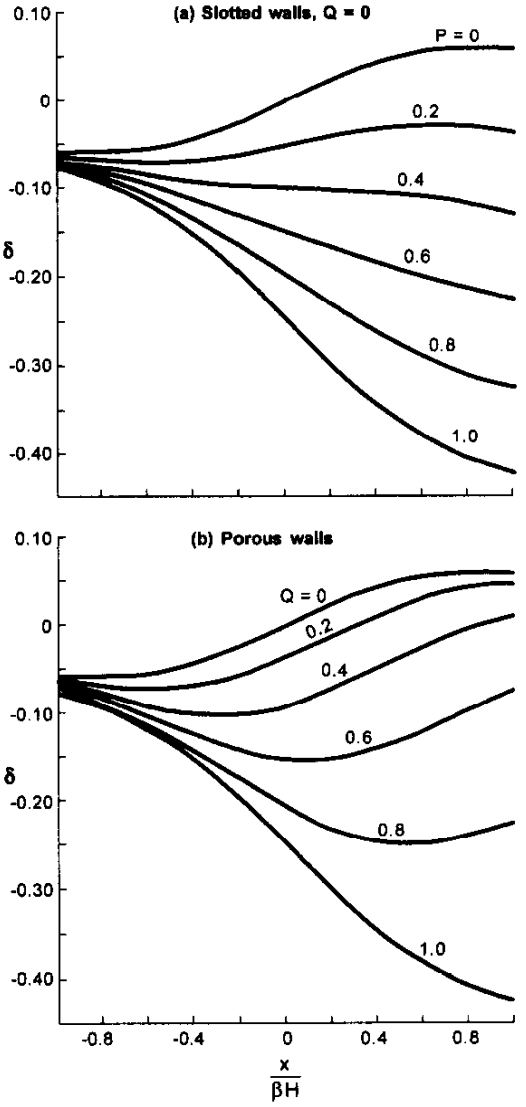

Figure 3.10 Longitudinal Variation of Upwash Interference in 2D Slotted and Porous Tunnels

3.3.2 INTERFERENCE OF SMALL MODELS, NONUNIFORM WALLS

The shortcomings of the ideal porous-wall boundary condition have long been recognised (see discussion in Sec. 3.2.2): the approximate nature of a linear crossflow boundary condition, the empiricism required to determine the crossflow resistance factor R for a given wall geometry, and the non-linear crossflow behaviour of real walls. The distinct flow physics of high total pressure flow out of the test section relative to low total pressure flow from the plenum into the test section suggests, at the minimum, a distinction between these flow regimes. The development of slanted-hole porous walls was instigated in part to balance inflow and outflow wall performance. Parallel developments in modelling walls with open slots explicitly recognised the different nature of re-entry flow from the plenum into the test section (Berndt [6]).

Such an approach has been applied, in an approximate way, to the NAE 15-in by 60-in 2D test section of the 5-ft by 5-ft Transonic Wind Tunnel (Mokry, Peake, and Bowker, [47]). For a lifting airfoil, it is proposed that the ceiling, or wall surface above the model, experiences predominantly inflow from the surrounding plenum because most of its extent will experience a pressure due to the model less than freestream static pressure (identified with the uniform plenum pressure). Conversely, the floor, with an imposed model pressure greater than plenum pressure (for the most part), will experience primarily outflow. Permitting each wall to have its own characteristic R may thus be expected to more accurately reflect the actual interference from these walls. Closed-form expressions are developed for interference quantities at the location of a small model (represented by a source doublet for volume and a point vortex for lift of an airfoil model at the centre of the tunnel). For equal upper and lower wall characteristics (and for a model centrally located), streamwise interference velocity at the model location is proportional to only the displacement effect of the model (doublet strength). Upwash interference velocity at the model is similarly dependent only on model lift (circulation). Allowing upper and lower walls to have different crossflow resistance factors (R_U and R_L) results in loss of this separability. For this more general case, streamwise interference velocity depends on both volume and lift, as does upwash. Interference factors are defined so that

$$\varepsilon = \frac{u_i}{U_\infty} = \Omega_s \frac{\pi}{6\beta^3}\left(\frac{c}{H}\right)^2 \frac{A}{c^2} + \Omega_\delta \frac{c}{H} C_L \tag{3.15}$$

$$\frac{w_i}{U_\infty} = \delta_0 \frac{c}{H} C_L + \delta_\Omega \frac{\pi}{6\beta^3}\left(\frac{c}{H}\right)^2 \frac{A}{c^2} \tag{3.16}$$

where Ω_s, Ω_δ, δ_0, and δ_Ω are analytic functions of R_U and R_L:

$$\Omega_s = 1 - \frac{3(t_U + t_L)}{2} + \frac{3}{2}\left(\frac{t_U + t_L}{2}\right)^2 - \frac{3(t_U + t_L - 1)}{4}\left[\cos\left(\frac{\pi(t_U + t_L)}{2}\right) - 1\right] \tag{3.17}$$

$$\Omega_\delta = -\frac{1}{8\beta}\sin\left(\frac{\pi(t_U - t_L)}{2}\right) \tag{3.18}$$

$$\delta_0 = -\frac{1}{4}\left\{\frac{t_U + t_L}{2} + \frac{1}{2}\left[\cos\left(\frac{\pi(t_U - t_L)}{2}\right) - 1\right]\right\} \tag{3.19}$$

$$\delta_\Omega = \frac{3}{2}\beta\left(\frac{t_U + t_L - 1}{2}\right)\sin\left(\frac{\pi(t_U - t_L)}{2}\right) \tag{3.20}$$

where t_U and t_L are defined as

$$t_{U,L} = \frac{2}{\pi}\arctan\left(\frac{R_{U,L}}{\beta}\right) \tag{3.21}$$

These interference factors are shown in Figure 3.11 as functions of Q_U and Q_L. For Q_U=Q_L the cross-coupling factors Ω_δ and δ_Ω are identically zero. Mokry et al. [47] report much better correspondence of measured wall pressures with predicted pressures for the best choice of distinct floor and ceiling porosity factors than is possible with equal wall crossflow factors.

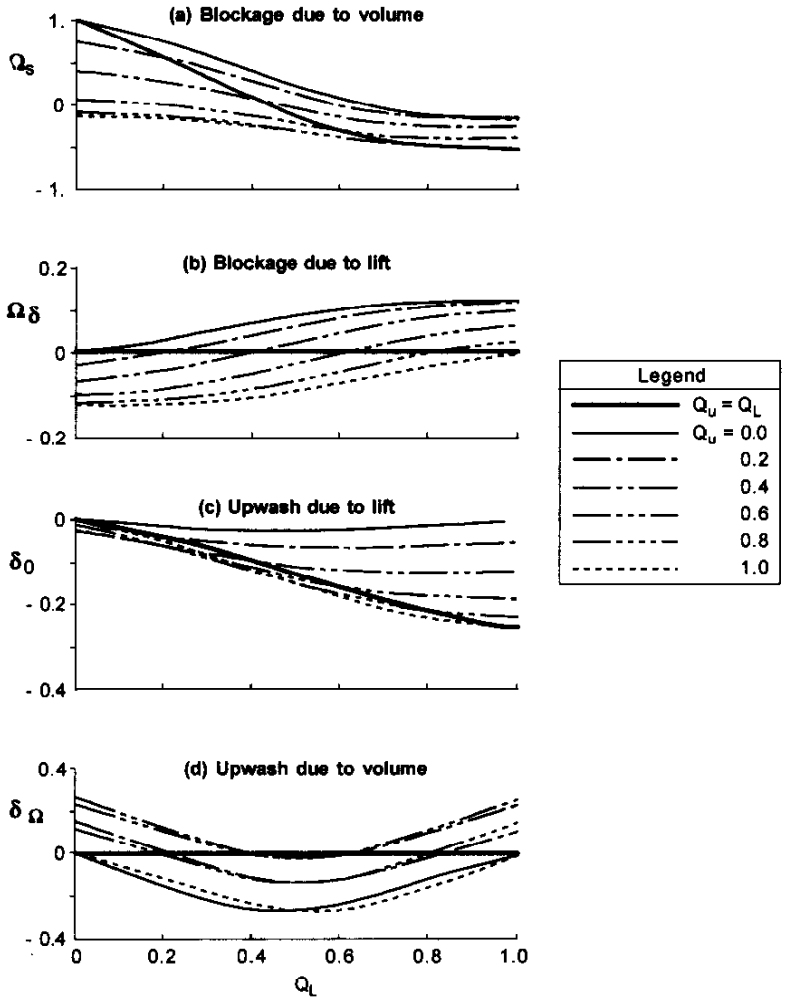

Figure 3.11 Interference in 2D Porous-Wall Tunnels With Different Floor and Ceiling Characteristics

3.4 INTERFERENCE IN 3D TESTING, CLASSICAL RESULTS

Techniques and methods for predicting the interference of a 3D model in a ventilated-wall test section parallel those used in two dimensions (with the obvious exception of complex variable methods).

The interference in ventilated-wall tunnels is characterised by the parameters defined by Equations 3.2 through 3.5: ε, δ, Ω_s, and δ_1. In 3D flow the blockage interference velocity ratio in a ventilated tunnel is thus given by

$$\varepsilon = \frac{\tau V \Omega_s}{\beta^3 C^{3/2}} \tag{3.22}$$

where Ω_s is a function of ventilated wall characteristics, τ is the tunnel shape factor, V is the effective model volume, and C is the area of the tunnel cross section. The wake blockage interference ratio, Ω_w, is similarly defined,

$$\varepsilon_w = \frac{\tau V \Omega_w}{\beta^3 C^{3/2}} \tag{3.23}$$

For small models centrally located in a test section with walls of uniform properties (i.e., constant coefficients in the ideal ventilated-wall boundary condition, Eq. 3.9) and with viscous and vortex wakes trailing straight downstream, symmetry considerations analogous to the 2D case confirm the decoupling of blockage and lift interference. That is, the streamwise interference velocity is due only to model volume and drag (the source singularities) and the cross-stream interference velocity (upwash) is due only to model lift. It can be expected that, just as for closed walls (Sec. 2.2) and for 2D porous walls (Sec. 3.3.2), this independence applies specifically to the model location. Interference velocity components at off-centreline locations, for models not centrally located, and for arbitrary distributions of wall properties may be due to both lift and blockage effects.

3.4.1 SLOTTED WALLS

Figure 3.12 shows the interference factors at the model location for small models in circular and rectangular wind tunnels with uniform homogeneous slotted walls. These data are compiled from AGARDograph 109 [24], Pindzola and Lo [53], and Holst [29]. The close correspondence of interference in circular and square test sections is expected.

A particularly simple analytic form approximates the lift interference of a small model in a circular slotted tunnel,

$$\delta_0 = \frac{1}{8}\frac{(F-1)}{(F+1)} \tag{3.24}$$

It is noted in AGARDograph 109 that this result is obtained both from the method of Baldwin et al. [3], whose solution for an infinitesimal span horse-shoe vortex is obtained by a Fourier transform method, and Davis and Moore [14], who give a solution for a finite-span horseshoe vortex (i.e., a uniformly loaded wing of zero sweep).

The solid blockage factor (Ω_s) changes only slightly with tunnel cross section because the closed tunnel reference blockage (through the tunnel shape factor τ) captures most of this influence.

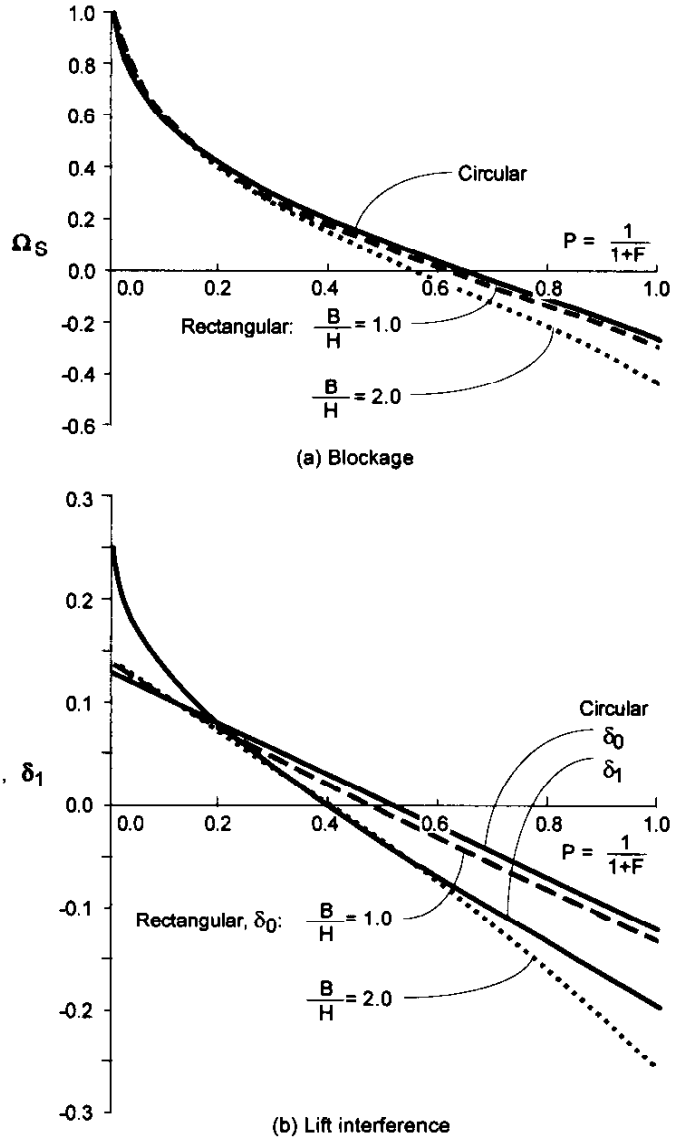

Figure 3.12 Interference of Small 3D Models in Ideal Slotted Tunnels

Lift interference, characterised by the interference factor δ, exhibits a larger variation with tunnel cross section. As discussed in Pindzola and Lo [53], for an ideal slotted tunnel the wake blockage interference is zero at the model (as well as far upstream) and the streamwise gradient due to solid blockage is zero (due to upstream and downstream symmetry of the blockage distribution). However, the streamwise gradient of wake blockage is not zero, resulting in a pressure gradient acting on the model, producing a force proportional to model effective volume. It is shown that for ideal slotted walls this gradient is identified with the magnitude of the solid blockage,

$$\frac{\partial \varepsilon_{wake}}{\partial x} = -\frac{C_D S}{2V} \varepsilon_{solid,closed} \Omega_s \tag{3.25}$$

Interference values for tunnels with just two slotted walls (typically the floor and ceiling) and two closed walls (sidewalls) are given by Pindzola and Lo [53], as well as for slotted tunnels with sidewalls having different slot parameters than the floor and ceiling.

3.4.2 Porous Walls

Figure 3.13 summarises the interference factors at the model location for small models in circular and rectangular wind tunnels with uniform ideal porous walls. These data are compiled from AGARDograph 109 (circular tunnel), Pindzola and Lo [53], and Lo and Oliver [43]. Just as for ideal slotted walls, the wake blockage gradient for ideal porous walls is given by Equation 3.25. Unlike slotted walls, however, ideal porous walls result in a non-zero streamwise gradient of solid blockage and in a non-zero wake blockage level. As discussed in AGARDograph 109 and elsewhere, wake blockage does not approach the classical closed wall result as porosity approaches zero. Mokry [46] explains this paradox as arising from the assumption that the walls are of infinite streamwise extent which results in discontinuous behaviour for the closed-wall case at upstream infinity. The importance of accounting for the proximity of the reference pressure measurement station to the model is emphasised, so that wake blockage is properly evaluated relative to the tunnel reference pressure location. Mokry [46] provides plots of streamwise variation of wake blockage for the 2D porous wall case. Lo and Oliver [43] provide similar distributions for 3D porous wall tunnels.

Pindzola and Lo [53] provide plotted interference parameters including streamwise distributions for porous wall tunnels having sidewalls of different characteristics than the floor and ceiling. Vaucheret [63] presents interference results for a test section with closed sidewalls and porous floor and ceiling. Appendices (in Vaucheret, [63]) document the equations used for application of the analytic Fourier transform method for 3D porous-wall tunnels with closed sidewalls and for a 2D porous-wall tunnel with different floor and ceiling characteristics.

Schilling and Wright [55] have calculated the upwash interference of finite-span horseshoe vortices (i.e., uniform wing loading) with span ratios of 0.3 and 0.7 in rectangular test sections with *B/H* from 0.5 to 2.0. Figure 3.14 summarises their results for the smaller span ratio. Closed-wall and open-jet results from Figure 2.5 (method of images) are shown for reference. Spanwise variation of interference is very small for the smaller span ratio; the larger span has substantially increased interference on the outboard wing.

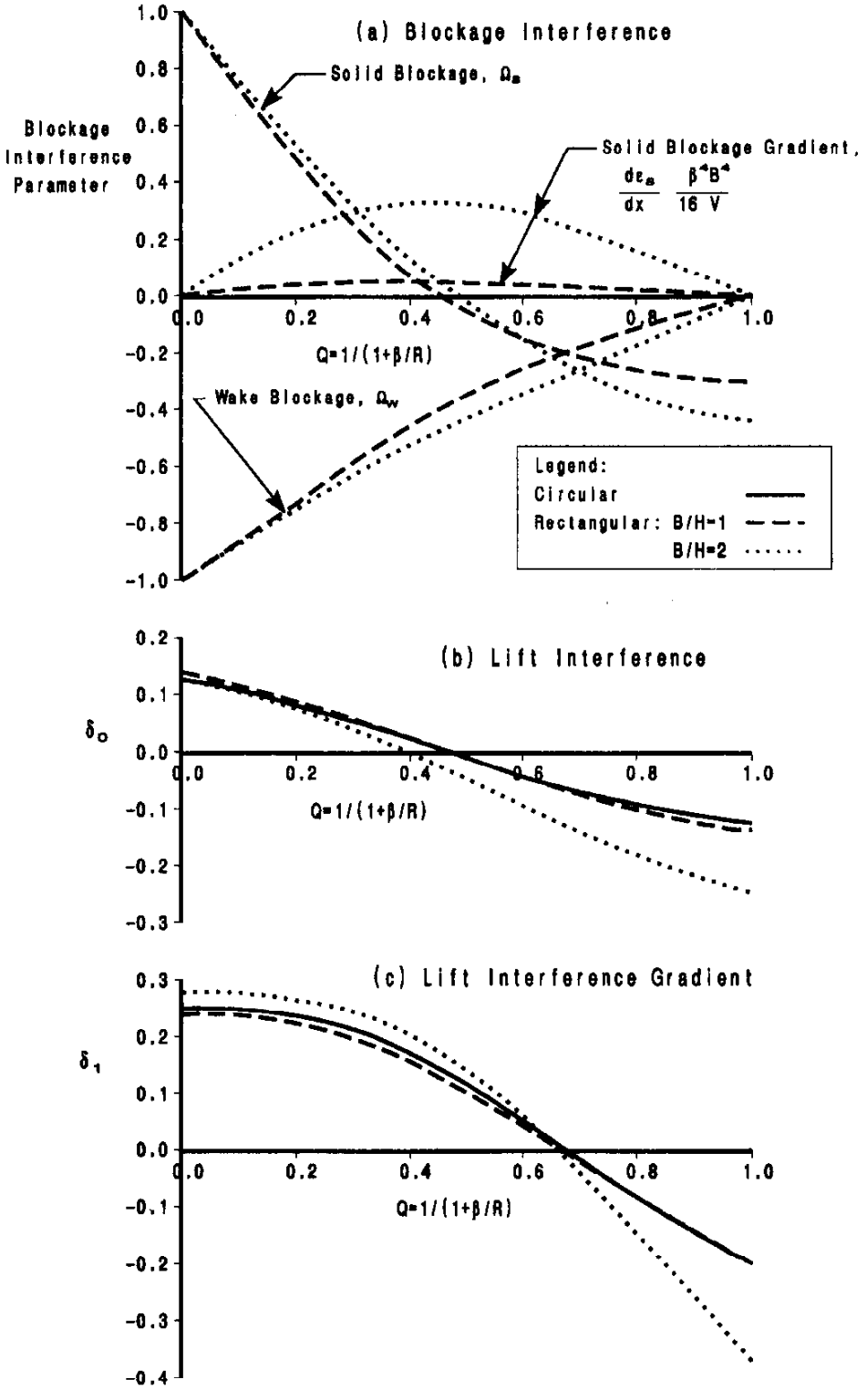

Figure 3.13 Interference of Small 3D Models in Ideal Porous Tunnels

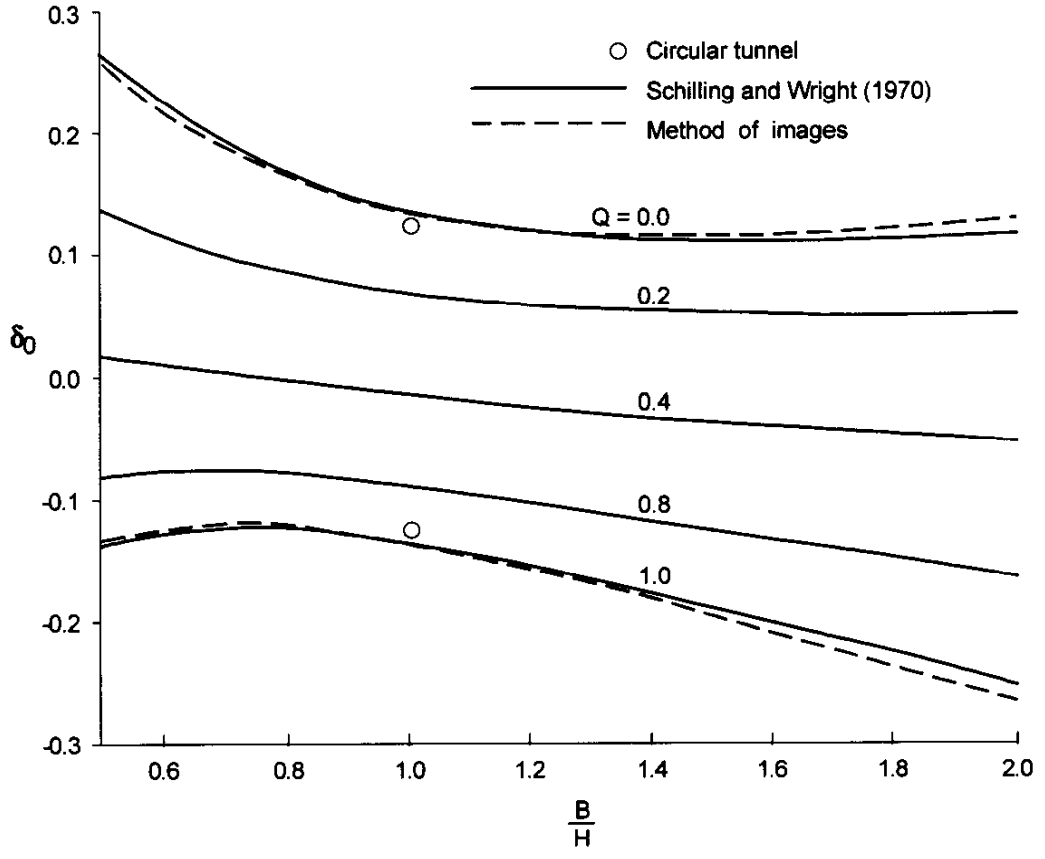

Figure 3.14 Lift Interference of Small 3D Wings in Ideal Porous Rectangular Tunnels

3.5 Computational Approaches to Interference Evaluation

The evolution of applied methods since the publication of AGARDograph 109 has generally followed the path from Fourier transform methodology (which forms the basis of results in Sec. 3.4), to panel methods with general analytic boundary conditions, and finally stepping to direct use of measured boundary conditions (see Chap. 4). An example of the latter approach is reported by Mokry, Digney, and Poole [50], who use measured wall pressures from a porous-wall transonic wind tunnel as specified boundary conditions in a panel code to assess wall interference. In general, the test article may be represented by either known or unknown singularity distributions, depending on model size, complexity, and accuracy requirements.

The principle of superposition states that the interference of collections of singularities is the sum of the separate contributions of each singularity. For a small model centrally located in a tunnel with uniform walls, this involves the solid blockage of the model volume distribution, lift interference from consideration of the model's lift (independent of volume distribution), and wake blockage from consideration of the viscous and separated wake drags. Use of singularities with strengths derived from gross model aerodynamics (volume, lift, drag) has the practical advantages of ease of use and bookkeeping simplicity. At the other extreme of model representation complexity, with a complex model geometry with many

unknowns, the analysis of a given configuration often proceeds by modelling the entire configuration and then extracting interference velocities and gradients (streamwise interference and upwash) without explicit identification with their separate origins in the classical sense.

3.5.1 POINT SINGULARITY MODEL REPRESENTATION

Keller and Wright [38] describe a panel approach for calculating the interference of lifting elements at arbitrary positions in ideal slotted (homogeneous) and porous rectangular test sections. A lifting wing is represented by a distribution of horseshoe vortices that can be located anywhere in the tunnel. Finite span, sweep, and arbitrary (specified) span loading can thus be modelled. Sample FORTRAN code is included both by Keller and Wright [38] and Keller [37]. The latter generalises the panel method to permit boundary conditions of the form

$$c_1\varphi + c_2\varphi_x + c_3\varphi_n + c_4\varphi_{xn} = 0 \qquad (3.26)$$

This permits investigation of slots with crossflow resistance, or so-called "viscous" slots, as well as ideal homogeneous slotted walls and ideal porous walls. The first term was used to investigate the integral form of the ideal slotted-wall boundary condition, leading to an understanding of the effect of finite tunnel length in the analysis: interference at the model stabilises to expected values when the tunnel starts about three tunnel widths upstream of the model. The effect of porosity in the slots is found to be large, as might be expected because the walls would behave like porous walls of equivalent $R=\tau R_{slot}$, where τ is the openness ratio of the slots, as long as the number of slots is not too small.

Parametric studies of interference in perforated wall tunnels (with closed sidewalls) are reported by Vaucheret [63]. Test section height to width ratio, wing span to width ratio, wing sweep, and horizontal wall porosity were investigated. Model representation and size limits are presented for keeping corrections below specified thresholds. Tunnel configurations for minimum interference are investigated in terms of horizontal wall characteristics, tunnel aspect ratio, and wing span. A similar set of results is given for a 2D porous test section with different floor and ceiling characteristics. An optimum 2D wall configuration for minimum interference is suggested as a closed floor (Q=0) and ceiling having Q=0.22.

The need for multiple singularities to represent the volume distribution of a typical model is demonstrated by Vaucheret [65] by consideration of wall pressure signatures, showing that 12 doublets adequately represent an ellipsoid (L/D=6) of 1% blockage in a square closed-wall tunnel, and that use of 30 doublets for a missile configuration provides a reasonable prediction of experimental pressures in a circular closed-wall tunnel. Similar calculated results for a single-doublet and a 20-doublet representation of the above ellipsoid are given for a square test section with porous walls, with significant differences in both blockage interference and blockage gradient, Figure 3.15. The method is extended to include wake blockage and support interference. Lift is represented by a flat vortex sheet, taking into account span, sweep, and span loading. Calculated wall pressures (at zero lift and increments due to lift) matched measured pressures best for a porosity factor of Q=0.2 (S3Ma wind tunnel). Sample calculations are also given for models mounted above or below tunnel centreline, highlighting the coupling of streamwise and upwash interference velocities with both model volume and lift.

WALINT, a wall interference code developed at the NASA Ames Research Centre (Steinle and Pejack [60]), uses point singularities to represent the model in rectangular slotted or porous test sections. Excellent agreement of upwash interference from WALINT and from the method of images for closed-wall and open-jet wall boundary conditions is shown. For the baffled slots of the Ames 11-ft Transonic

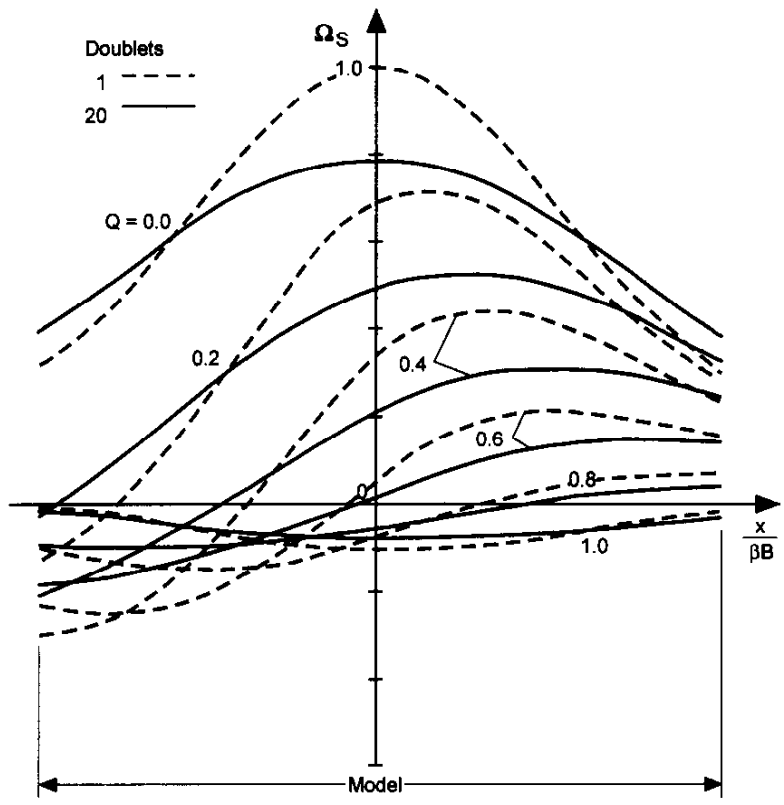

Figure 3.15 Effect of Model Representation on Solid Blockage of an Ellipsoid (L/D = 6, blockage = 1%) in a Square Ideal Porous Tunnel with Closed Sidewalls (Vaucheret [65])

Wind Tunnel, a value of R=19 is quoted. Because there are many slots (54 total on four walls), in the limit of large R (no crossflow resistance) the calculated interference of the walls with discrete slots should be very similar to that of ideal homogeneous slotted walls. The ideal inviscid slot results for a rectangular tunnel with closed sidewalls are essentially duplicated by WALINT using R/β=10,000. The interference equivalence of homogeneous porosity and porous strips is demonstrated, with identical upwash interference for a lifting element located within the central region of the test section (|y/B|<0.3). Steinle and Mabey [59] report computed interference results from WALINT using 20 singularities to represent an elliptically loaded wing with a span to tunnel width ratio of 0.7. Twelve source doublets were used to represent a model body whose length equals the wing span. For the cases analysed the spanwise variation of interference upwash was much less for slots with resistance than for ideal slots.

3.5.2 Panel Methods, Homogeneous Ventilated Walls

Most recent computations of wall interference rely on panel or vortex lattice computational methods. Vaucheret [66] reports results from a vortex lattice code used to overcome restrictions of classical analytical methods regarding geometry of the test section (both in cross-section and streamwise extent), model and sting incidence, and wall boundary conditions. A model and its support system may be represented by either a collection of singularities of strengths determined by the known geometry and loading, or by panels with unknown strengths. For a closed-wall case, inlet conditions were uniform to within $Cp<10^{-5}$ when the test section length was at least seven times the tunnel height. Use of a non-

linear porous-wall boundary condition is compared to results with a linear crossflow wall characteristic. The addition of perforated window inserts in the closed sidewalls of a test section with perforated floor and ceiling (S2 tunnel) is shown to decrease both the spanwise and chordwise variation of upwash interference for a transport model. The effects of model proximity to reference static pressure taps are shown for the S1Ma tunnel. It is suggested that not more than 6000 mesh cells be used per half-configuration (i.e., for problems with one plane of symmetry and including a support that requires panelling). For a simple case, however, it is reported that the upwash correction in a cylindrical test section is essentially the same for solutions with 270 and up to 5600 panels.

PAN AIR, a higher order panel code for linearised potential flow analysis (Magnus and Epton [45]) as well as TRANAIR, which solves the full potential equations (Johnson et al. [35]), have been used to investigate interference in the Ames 11-ft Transonic Wind Tunnel. Tunnel modelling has mainly been limited to long tunnels with constant wall properties. Computational tunnels typically extend two or more model lengths upstream and downstream of the model. The model in the test section is a part of the input geometry; the singularity strengths associated with its panelling are unknowns along with the wall panel strengths. The effect of the walls on model loading is thus an explicit part of the solution. The walls were modelled as homogeneous ideal porous walls with R=1.14, corresponding to R=19 for the baffled slots (at 6% openness) as recommended by Steinle and Pejack [60].

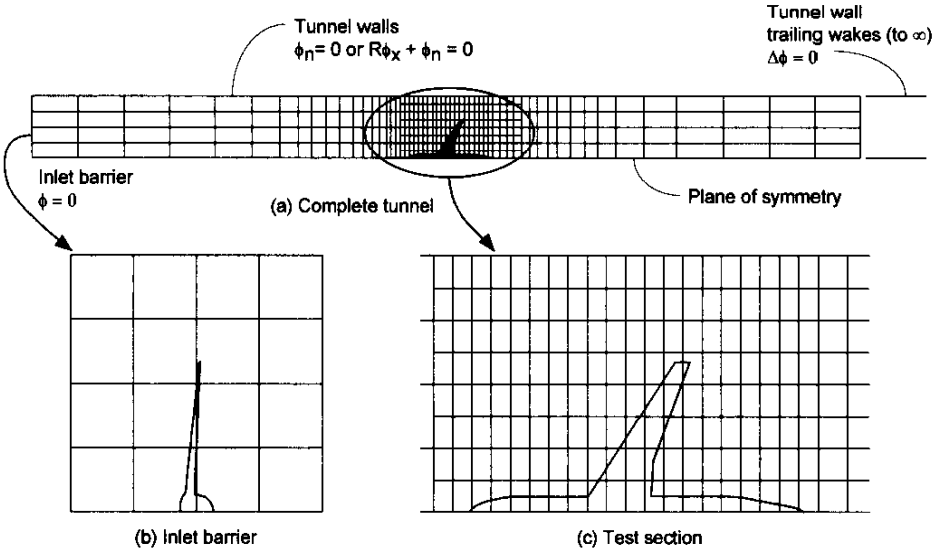

Figure 3.16 Typical Panelling with Boundary Conditions

Figure 3.16 depicts a typical panelling and associated boundary conditions for the analysis of a floor-mounted half-model with ideal homogeneous porous walls. The floor is not panelled because it is treated as a plane of symmetry in the analysis. Approximately 2000 panels are used: about 1000 for the wind tunnel walls, the remainder for the model. It was found that doubling the panelling had a negligible effect on the interference. This panelling exhibits several features characteristic of this type of analysis. The tunnel is very long so that flow perturbations due to the model are negligible before the ends of the computational tunnel are encountered (except for the trailing vortex wake at the downstream end; no viscous wake was included in this analysis). Wall panel size is varied to adequately capture streamwise and circumferential variations of the pressure field due to the model. Far upstream where pressure gradients are small, large panels are sufficient. In the region around the model, streamwise panel

spacing is decreased significantly and circumferential panel density is doubled. No leakage problems have been encountered. Inflow through the upstream face equals outflow at the downstream end of the tunnel as long as the walls are long and have constant ideal characteristics.

Good agreement with wall pressures measured between the slots have been obtained. Calculated interference for several transport models, Figure 3.17 (Goldhammer and Steinle [28]) exhibits differences in lift interference attributable to differences in both wing span and sweep. Blockage interference is small and essentially the same for these models. The spatial variation of interference for the largest of these wings at a cruise condition is illustrated in Figure 3.18. A root-to-tip Mach increase of 0.005 represents the streamwise gradient of blockage due to porous-wall crossflow characteristics. Upwash interference variation over the wing planform is only slightly larger than 0.02 degree.

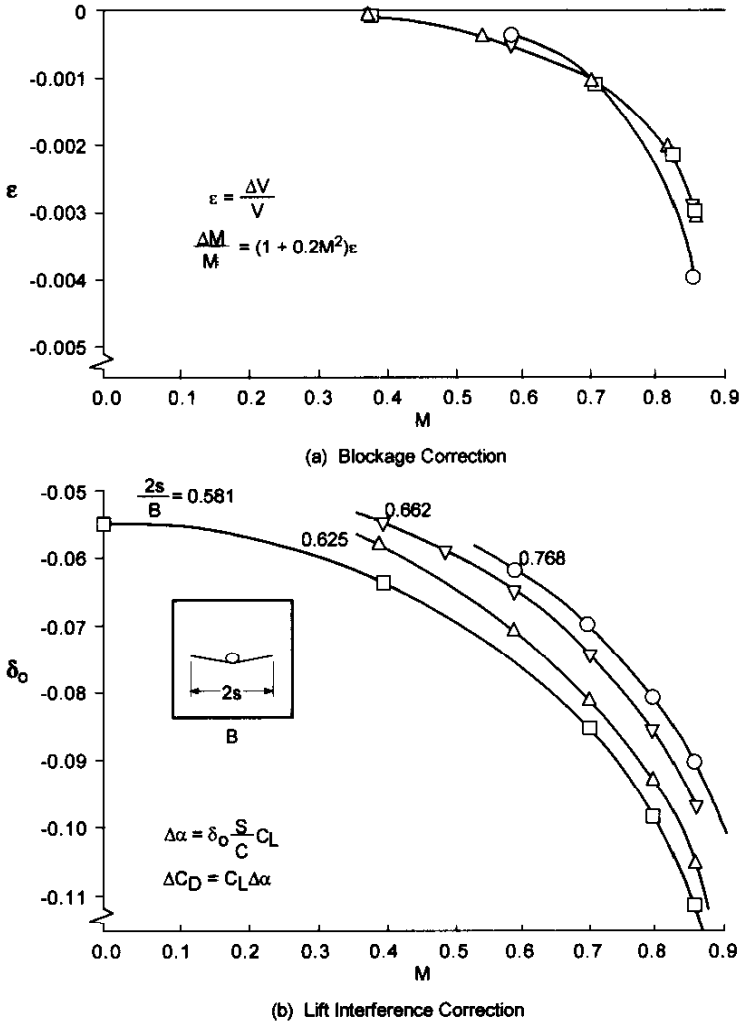

Figure 3.17 Interference at the Wing Reference Location for Transport Half-Models in an Ideal Porous-Wall Tunnel; R=1.14, B/H=2.0, M = 0.80, $C_L \cong 0.45$ (Goldhammer and Steinle [28])

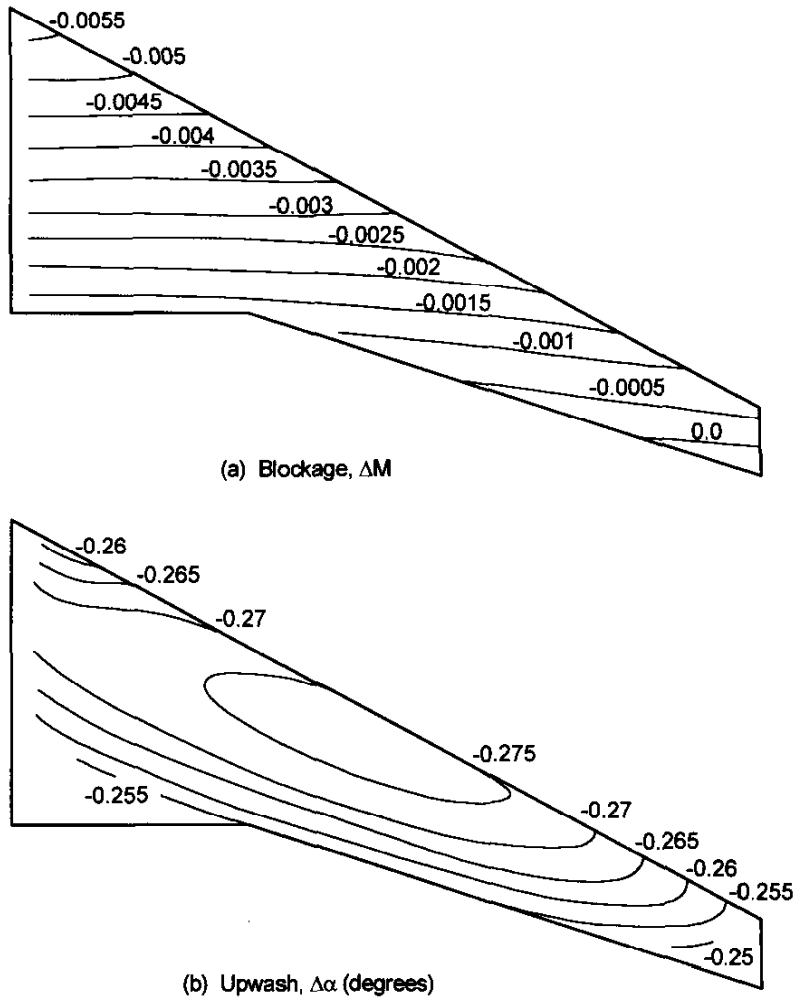

Figure 3.18 Interference Distribution at the Wing in an Ideal Porous-Wall Tunnel: R = 1.14, B/H=2.0, M = 0.8, $C_L \cong 0.45$, 2s/B=0.768 (Goldhammer and Steinle [28])

3.5.3 Panel Methods, Finite-Length and Discrete Slots

Two geometric features that differentiate all real test sections from the idealised tunnels of the preceding sections are discreteness of wall ventilation and finite upstream and downstream extent of wall ventilation. Related to the latter are the further considerations of model support struts and test section diffuser interference at the downstream end of the test section, as well as possible entrance effects due to proximity of the contraction at the upstream end of the test section.

Generally the importance of these elements may be discounted as distance from the disturbance source (in hydraulic diameters) increases beyond one. This is hardly ever the case at the downstream end of the test section where a combination of a closed-wall diffuser, a large support strut, and possibly re-entry plenum flow often occurs within a hydraulic diameter from the end of the model. The issue of discreteness of wall openings arises in two general contexts: interference of walls with a small number of slots and the implications of wall flow details on measurement methods (Chap. 4).

Kemp [39] [40] has developed a numerical method of a slotted wind tunnel test section using a general-purpose panel program as a starting point. Model lift and volume distribution can be represented by singularities with specified strengths. Walls are modelled using superposed source and doublet panels, Figure 3.19. The homogeneous ideal slot boundary condition (in integral form) may be specified for the

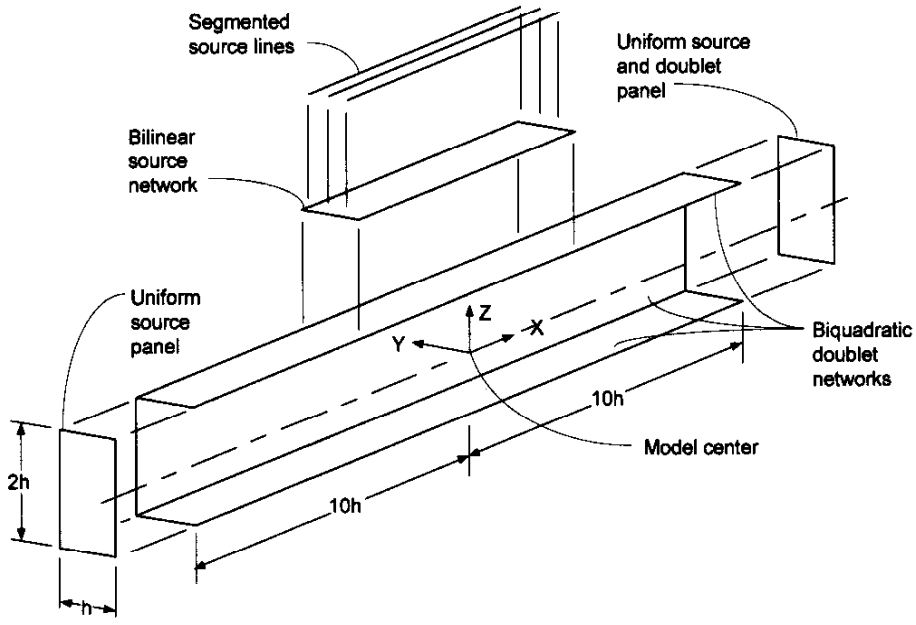

Figure 3.19 Tunnel Modelling (Kemp [40])

walls. Discrete slots are modelled by the addition of source lines to gather the distributed mass flux through the wall. Consideration of flow in the crossflow plane toward a single slot suggests that within a slot spacing from the wall the flow is the same as for the equivalent homogeneous slotted wall. Investigation of non-linear slot boundary conditions (including a quadratic crossflow term and an approximation to the slot inflow model developed by Berndt and Sorensen [8]) found significant streamwise interference due to lift for a model in the centre of the tunnel. Calculation of interference for slots of finite length ($-1.58<x/H<1.46$) resulted in unbalanced massflow through the tunnel. The walls were initially found to provide a net inflow to the tunnel. Balanced inflow and outflow was achieved by letting the plenum pressure in the slotted-wall boundary condition be different from the upstream reference pressure. In effect, the plenum is numerically depressurised until it no longer pushes a net inflow into the test section.

For tunnels of infinite upstream and downstream extent and with constant coefficients in the ideal boundary condition, integration of Equation 3.9 in x from far upstream to far downstream results in zero net mass flux through the walls (as long as φ, the perturbation potential of the model, goes to zero at these limits). Any other streamwise distribution of wall properties, R and K, or nonlinearity of the boundary condition (as noted by Kemp, see above) can be expected to result in a tunnel exit flow which does not equal the entrance flow. The walls may either add or extract flow from the tunnel. The strategy of adjusting plenum pressure in the ventilated-wall boundary condition must be applied for each particular flow condition for a given model. Pressure and force coefficients computed using upstream flow conditions must be recalculated to reflect the plenum static pressure and its associated Mach number as the proper reference conditions. This parallels the common operating primacy of plenum static pressure in real ventilated-wall tunnels.

The effect of finite slot length on the interference of the three basic point singularities is shown in Figure 3.20 (from Kemp [40]). Closed-wall interference is shown for reference. For solid blockage, Figure 20a, blockage at the model location for the two slotted-wall cases is in agreement if the reference static pressure is taken as plenum pressure (represented by the parameter u_p) for the finite-length slot case. In Figure 20b, the case with plenum suction (for offsetting wake blockage) demonstrates decreases in both wake blockage and wake blockage gradient at the model location. Lift interference at the model location is affected very little by the finite extent of the slots or by the numerical simulation of a re-entry flap at the trailing edge of the test section, Figure 20c. Depending on the size of the model, however, upwash at the tail may be affected.

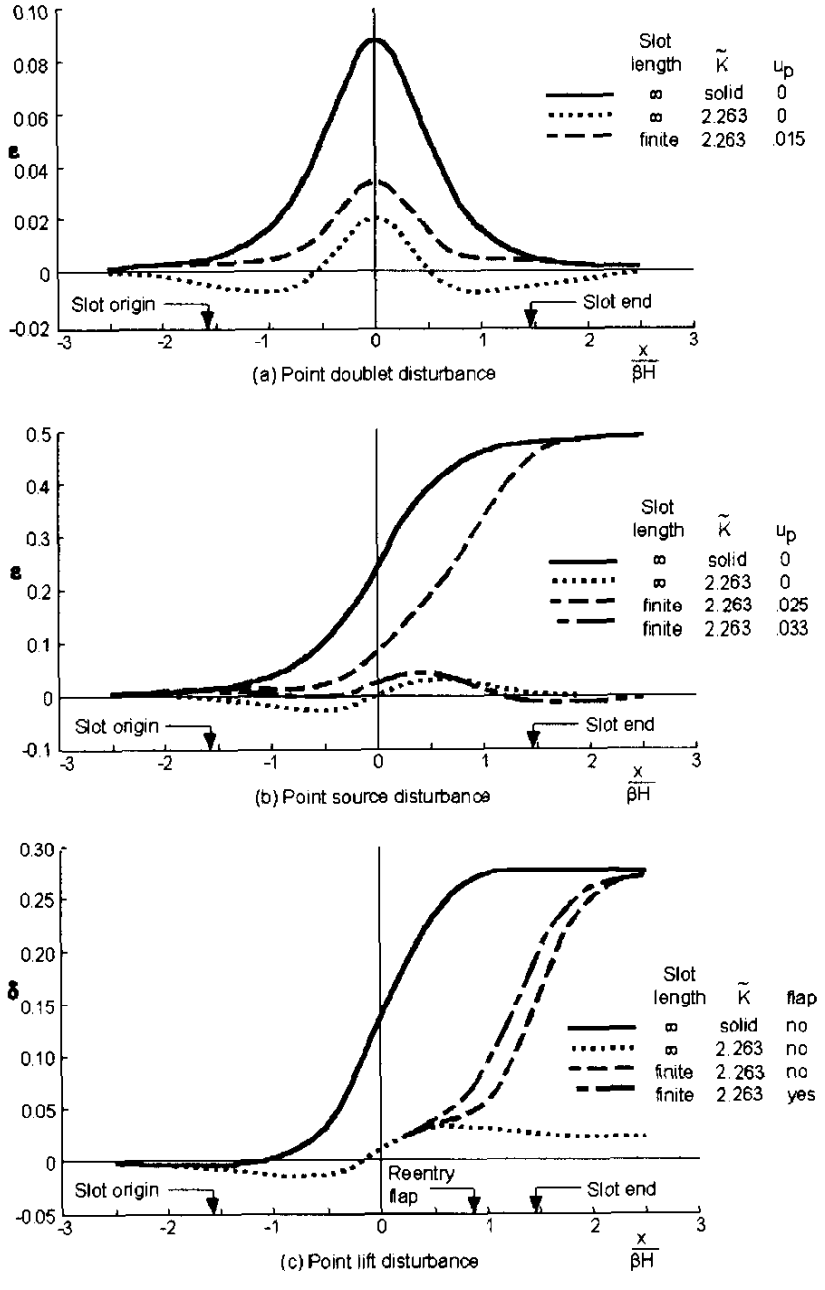

Figure 3.20 Effect of Finite Length of Slots on Interference (Kemp [40])

The evolution of wall correction methodology as applied to a production transonic wind tunnel is exemplified by developments at the Boeing Transonic Wind Tunnel (BTWT). Operation as a high-subsonic wind tunnel began in 1944 with conversion to transonic capability in 1953, including the installation of slotted walls. The test section has an 8-ft by 12-ft rectangular cross section with 2-ft corner fillets. The walls have 16 longitudinal slots at a nominal openness of 11%. Panel code interference calculations (Lee [42]) using the ideal homogeneous slotted-wall boundary condition (Eq. 3.9 without the viscous term) for a moderately sized model ($2s/B<0.6$) corresponded very closely to the classical value, $\delta_0=-0.11$ (Davis and Moore [14]) for lift interference. Calculated blockage corrections were so small as to be considered unverifiable.

An example where discrete slot modelling was found necessary is shown in Figure 3.21. The closed-wall corner fillets at the BTWT floor intrude into the flow field of a floor-mounted half-model at its plane of symmetry. Although details of the flow through the slots are not expected to be well represented in this inviscid calculation, comparison of calculated wall pressures to measurements provides some clues regarding slotted-wall behaviour for this tunnel. Increasing magnitude of the pressure peak due to wing lift (section K in Fig. 3.21) is expected with increasing wall resistance (R decreasing). Movement of the pressure peak (due to lift) downstream is also associated with decreasing R. Decreasing the slot width, consistent with the slot-flow model of Berndt and Sorensen [8] would be expected to improve this aspect of the correlation. The resistance of the slots improves the wall pressure correlation on the pressure side of the wing as well, though the more meaningful metric is the pressure difference between opposite walls (an error or bias in reference Mach number or static pressure would be manifested as a C_p zero shift). Although the longitudinal extent of pressures is limited, upstream values suggest an asymptotic approach to a non-zero C_p. This is consistent with the previous discussion relating to plenum pressure lower than upstream static pressure for finite-length wall ventilation. Finally, even though the downstream range of pressure measurements is very limited, there is some indication of a longitudinal gradient in the measurements that is not present in the theoretical models. This is thought to be related to non-ideal slot behaviour. The proximity of the unventilated fillets has the effect of shifting the interference toward more closed-wall values relative to the equivalent homogeneous-wall tunnel, Figures 3.22 and 3.23.

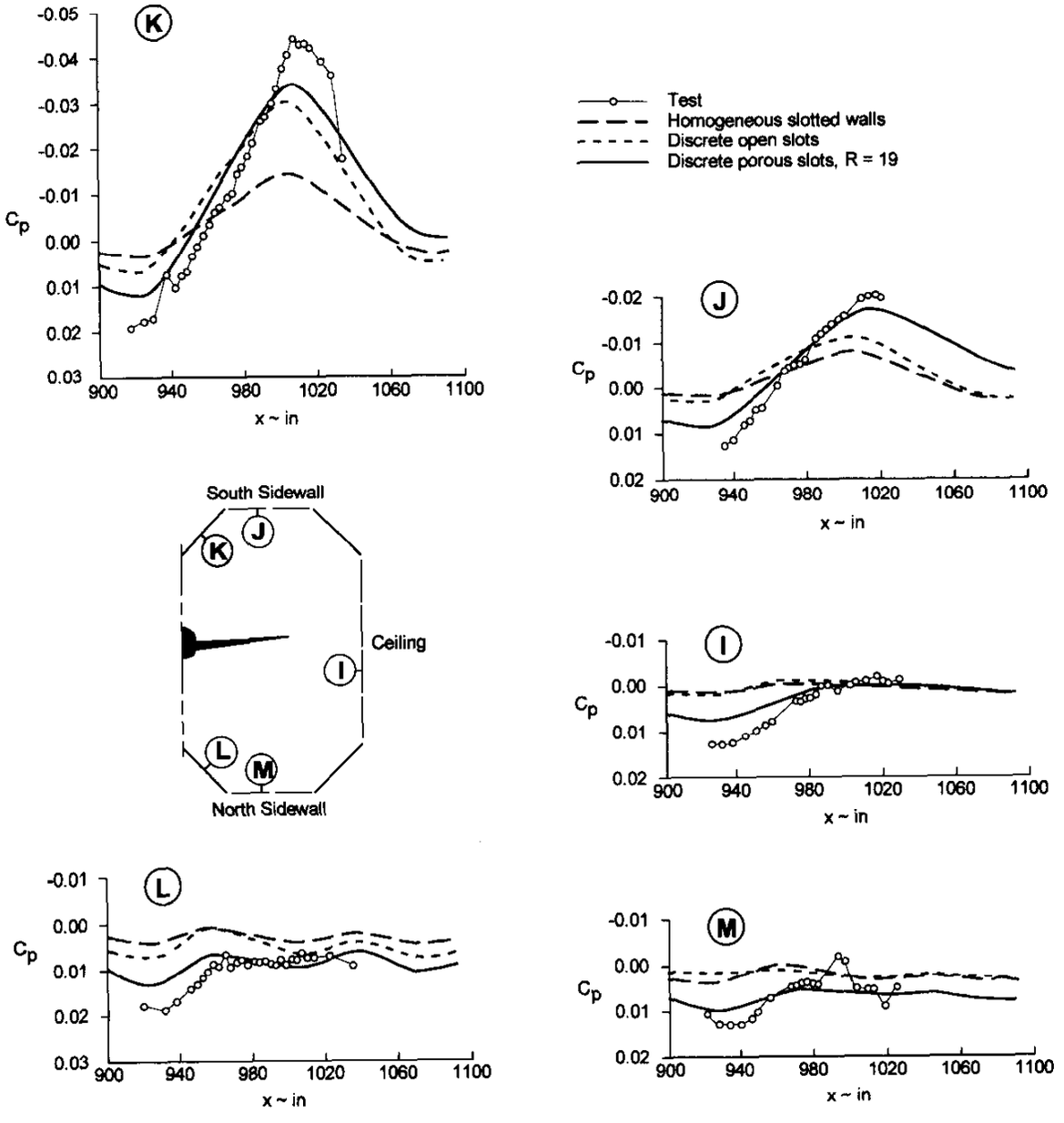

Figure 3.21 Wall Pressures in a Slotted-Wall Tunnel with a Transport Wing-Body Half-Model, M = 0.8, $C_L \cong 0.45$

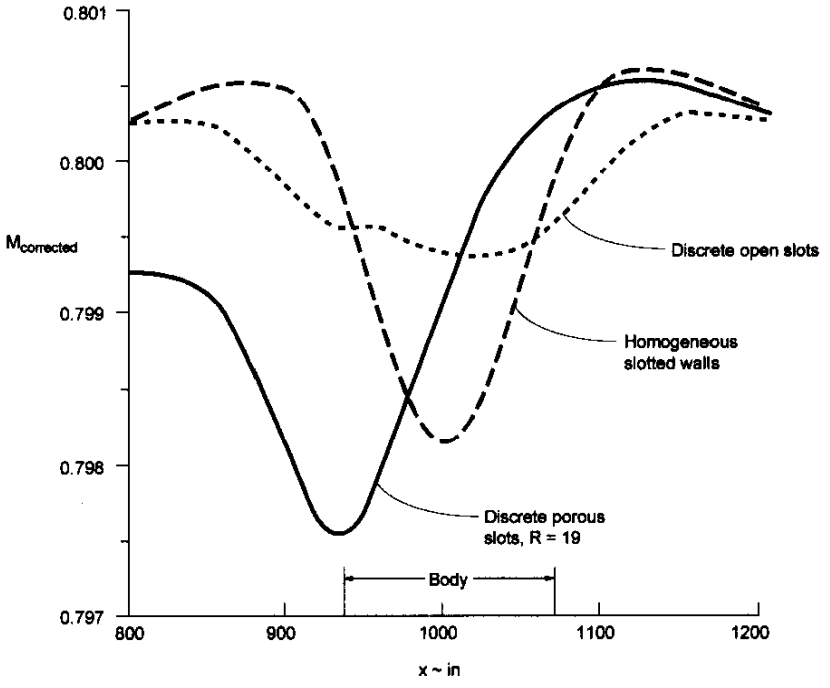

Figure 3.22 Longitudinal Distribution of Blockage Interference of a Transport Half-Model in a Slotted-Wall Tunnel, M = 0.8, $C_L \cong 0.45$

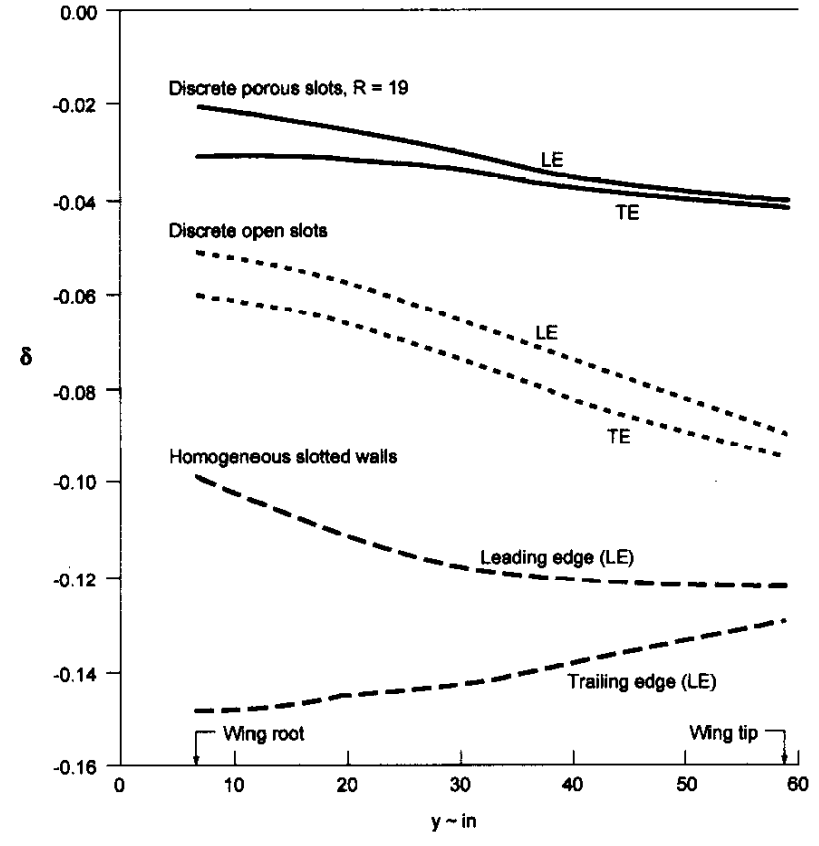

Figure 3.23 Spanwise Variation of Upwash Interference of a Transport Half-Model in a Slotted-Wall Tunnel, M = 0.8, $C_L \cong 0.45$

Continuing concern over the proper slotted-wall boundary condition has been addressed by a series of wall interference investigations in which typical sting-mounted transport wing-body models have been tested and analysed in BTWT with two different wall configurations: closed walls and 11% open slots. Code predictions of the interference in the closed-wall test section were used to correct the measured force data. These interference-free data were used to deduce lift interference of the slotted walls. Assuming that blockage and flow curvature corrections are small in the slotted test section, the lift interference factor for slotted walls is calculated from the interference-free (closed-wall measurements, corrected using CFD upwash and blockage) and uncorrected (slotted-wall measurements) lift-curve slopes,

$$\delta_0 = \frac{C}{S}\left[\frac{1}{a_{corr}} - \frac{1}{a_{unc}}\right] \tag{3.27}$$

In parallel to the experimental efforts, the wall boundary conditions were varied computationally with the goal of matching wall pressures measured midway between wall slots both above and below the model. The wall pressure data quality is considerably improved by first subtracting clear-tunnel distributions. The resulting pressures are then interpreted as being due to only the model and its sting support. Further conditioning of the wall data is done by fitting each wall pressure measurement (the i-th tap) in a least-squares sense in C_L (up to 0.45) at each Mach number:

$$C_{p_i} = CP0_i + CP1_i \times C_L \qquad (3.28)$$

where *CP0* is the model signature at zero lift and *CP1* represents the incremental effect of model angle of attack. Figure 3.24 compares the experimentally determined coefficients to CFD predictions for the closed-wall configuration. The better correlation of the full potential code with experiment reflects the role of non-linear compressibility in the flow. For the slotted-wall configuration, various ventilated-wall boundary conditions have been investigated: ideal homogeneous slots, discrete slots with an open-jet (constant pressure) boundary condition, constant ideal porosity applied at the slots, and several combinations of variable porosity. The variable-porosity wall models are motivated by physical considerations: the volume of the pressure plenum below the floor is restricted by a large external force balance and its associated enclosure. Figure 3.25 compares measured wall pressure for the slotted walls to CFD calculations for walls with R=10 for the floor slots and R=18 for the remaining slots.

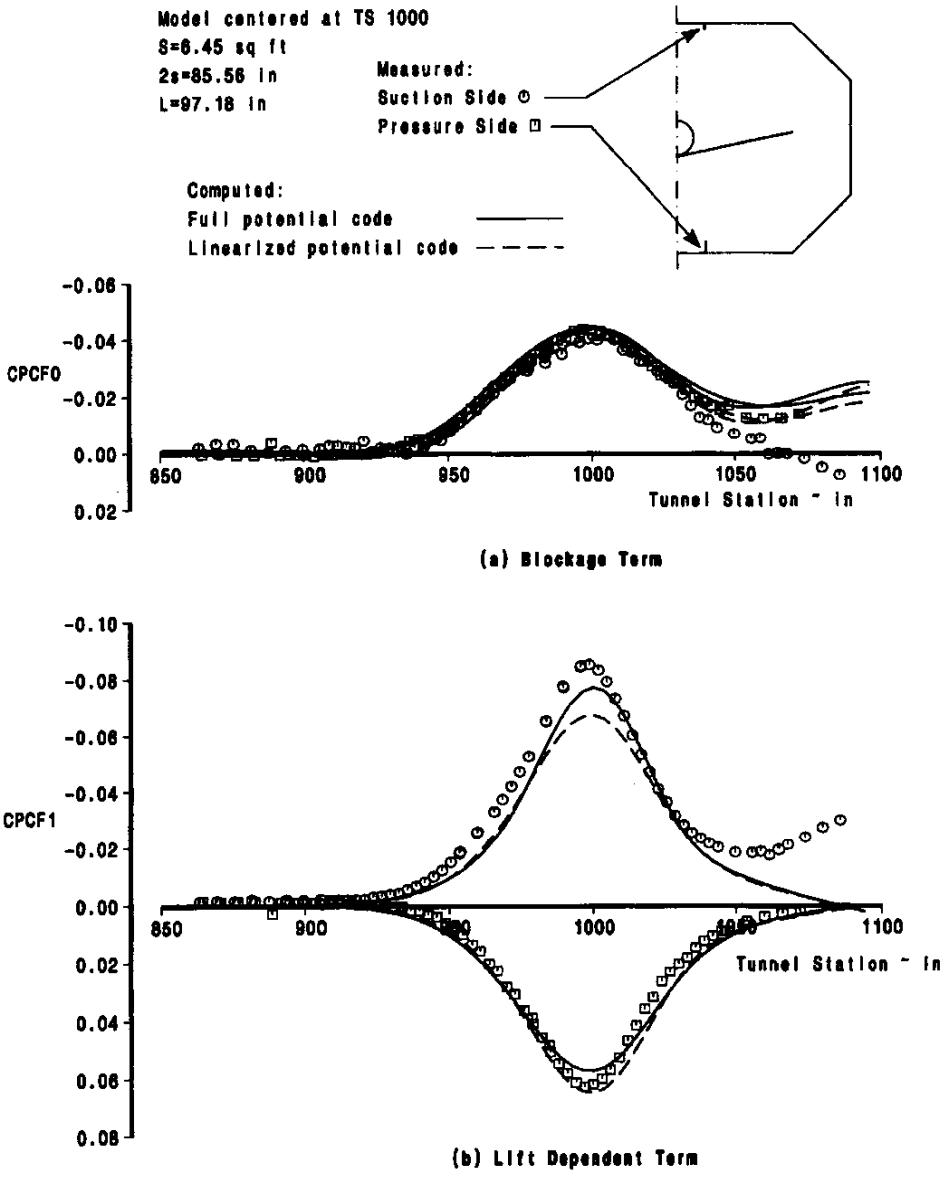

Figure 3.24 Computed and Measured Wall Pressures with Closed Walls
767-300 Wing-Body at M = 0.80

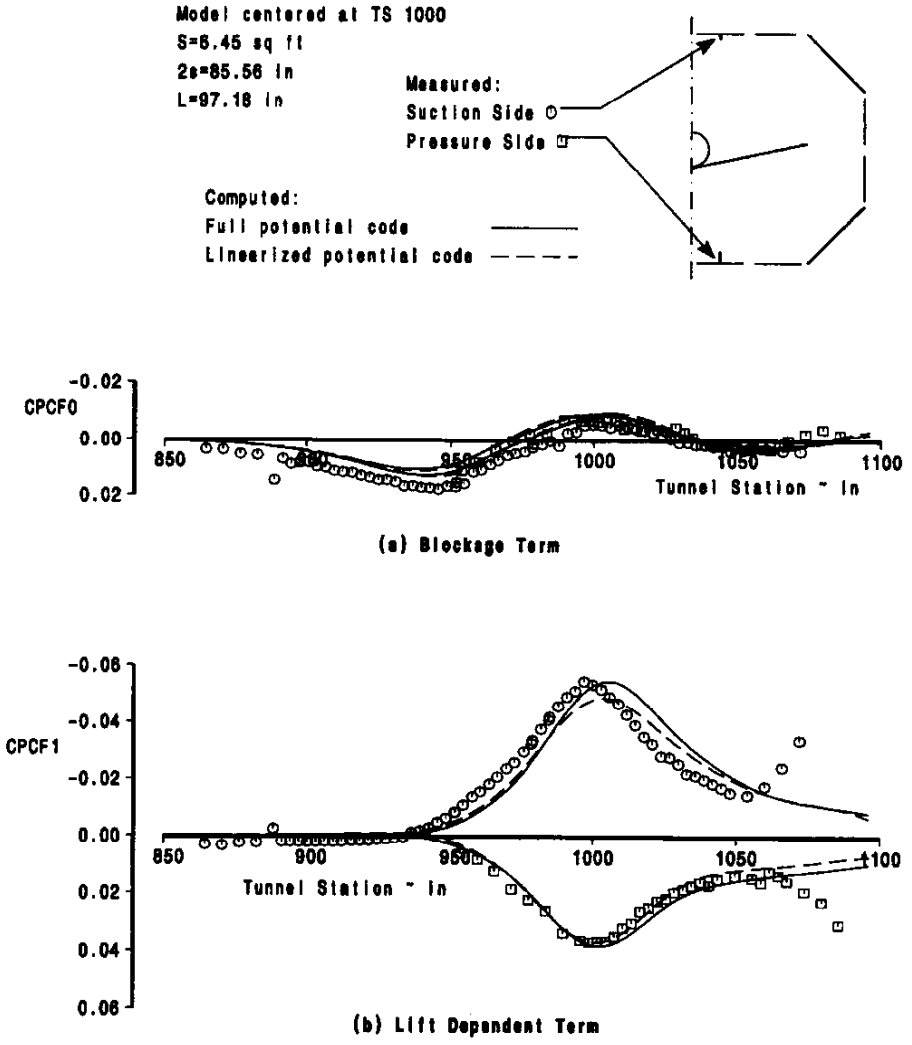

Figure 3.25 Computed and Measured Wall Pressures with Slotted Walls 767-300 Wing-Body at M = 0.80

The interference factors deduced from these studies are shown in Figure 3.26. The Mach number correction for closed walls from the linear potential code shows no variation of blockage interference with model attitude. The full potential code indicates similar interference at zero lift (α = -2 deg), but slightly increased blockage with angle of attack. The variation of δ_0 with Mach number for the experimental data suggests that the slot characteristics include some measure of porous-wall behaviour (for which interference factors depend on R/β). The irregularity for $M > 0.80$ is thought to be due to uncertainty in the blockage correction used to correct the closed

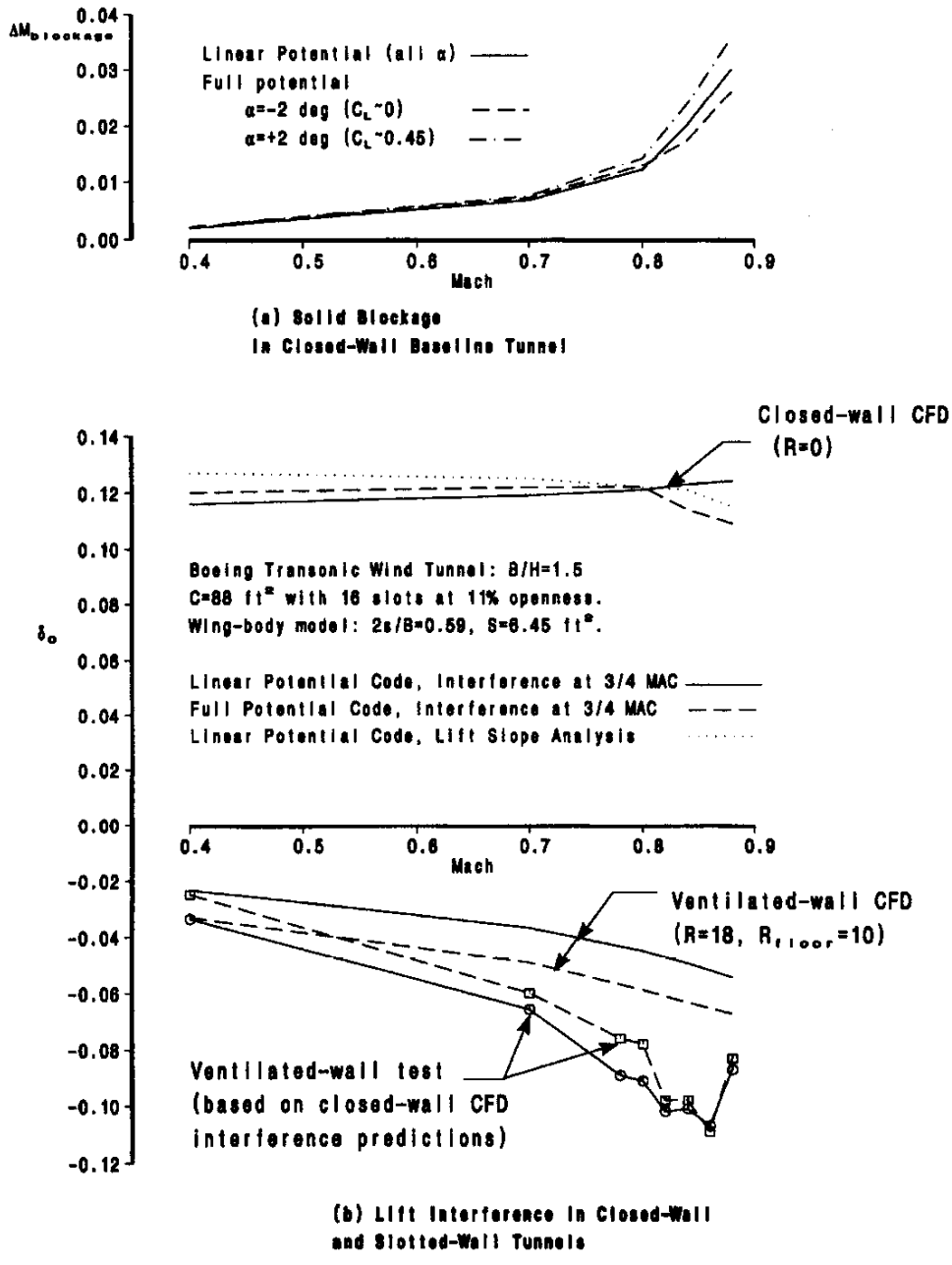

Figure 3.26 Interference of a Subsonic Transport Model in a Slotted-Wall Tunnel

wall data at high-subsonic Mach numbers. An error in the blockage correction factor (ε) for closed walls of 0.001 corresponds to a dynamic pressure correction ratio of 1.002, which directly scales the measured lift curve slope. At M=0, this corresponds to a numerically equivalent change in δ_0 of approximately 0.01. An error of this magnitude for incompressible solid blockage is magnified fourfold at M=0.84. This source of uncertainty is present in both the closed-wall interference value and in the assumption of negligible slotted-wall interference. Uncertainties in δ_0 are due to both sources . This interdependence of extracting two or more interference components from a single set of data having unknown interference suggests that increasing accuracy requirements on one component be matched by corresponding accuracy for the others, including the accuracy of the "interference-free" data set.

The distribution of blockage and upwash interference at the wing at M=0.80 for closed walls and the differential resistance wall model is shown in Figure 3.27. These results support the initial assumption of negligible blockage interference and demonstrate a significantly smaller variation of upwash interference over the wing planform for slotted walls compared to closed walls.

An investigation of wall and slot geometry in support of slotted transonic tunnel development efforts considered the effect of slot number on interference. The slotted-wall boundary conditions for this study combine adjacent columns of panels with either an open-jet or closed-wall boundary condition. Figures 3.28 and 3.29 compare interference at the model station (x=2000 in) for two cases of equivalent total slot openness (10%): 4 slots (2 on each of the floor and ceiling) and 24 slots (6 on each of the floor and ceiling, 4 on each sidewall). Larger spanwise gradients of both blockage and lift interference are evidently due to the closed sidewall. Longitudinal gradients of interference at the tunnel centreline are very similar, Figure 3.29. Another tunnel development study using a porous-slot boundary condition (Bussoletti et al. [10]) indicates that interferences at the model for a large number of slots and for equivalent homogeneous walls are very similar, Figure 3.30.

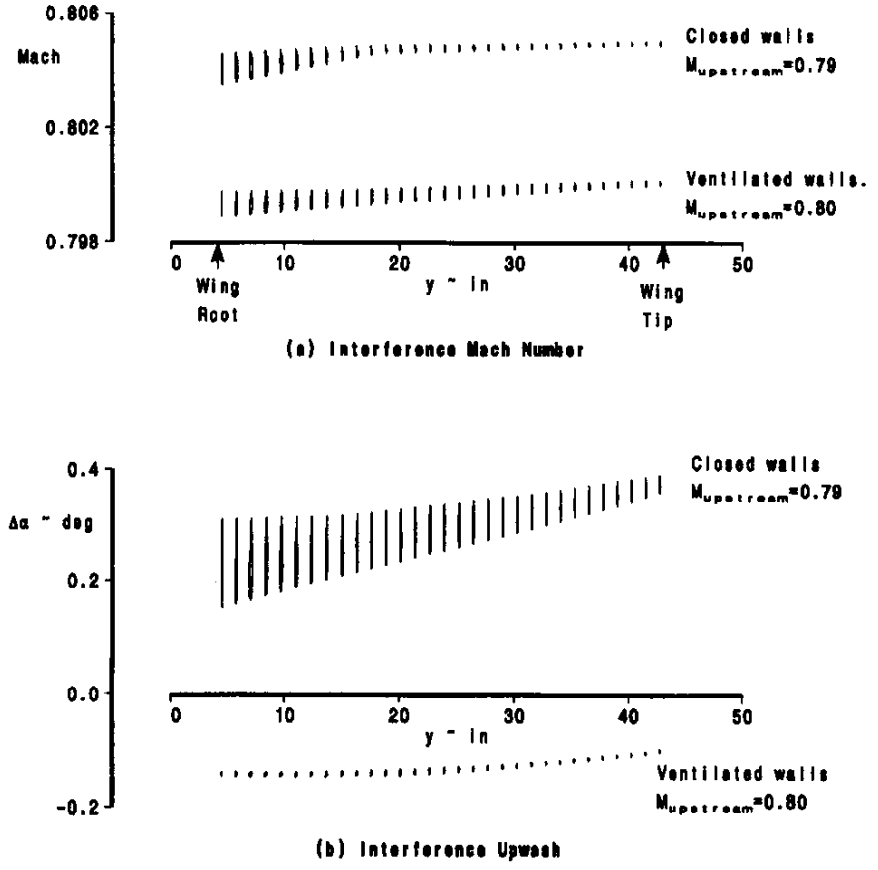

Figure 3.27 Interference at the Wing of a Transport Model in Tunnels with Closed and Ventilated Walls, 2s/B = 0.594, $C_L \approx 0.45$, B/H = 1.5

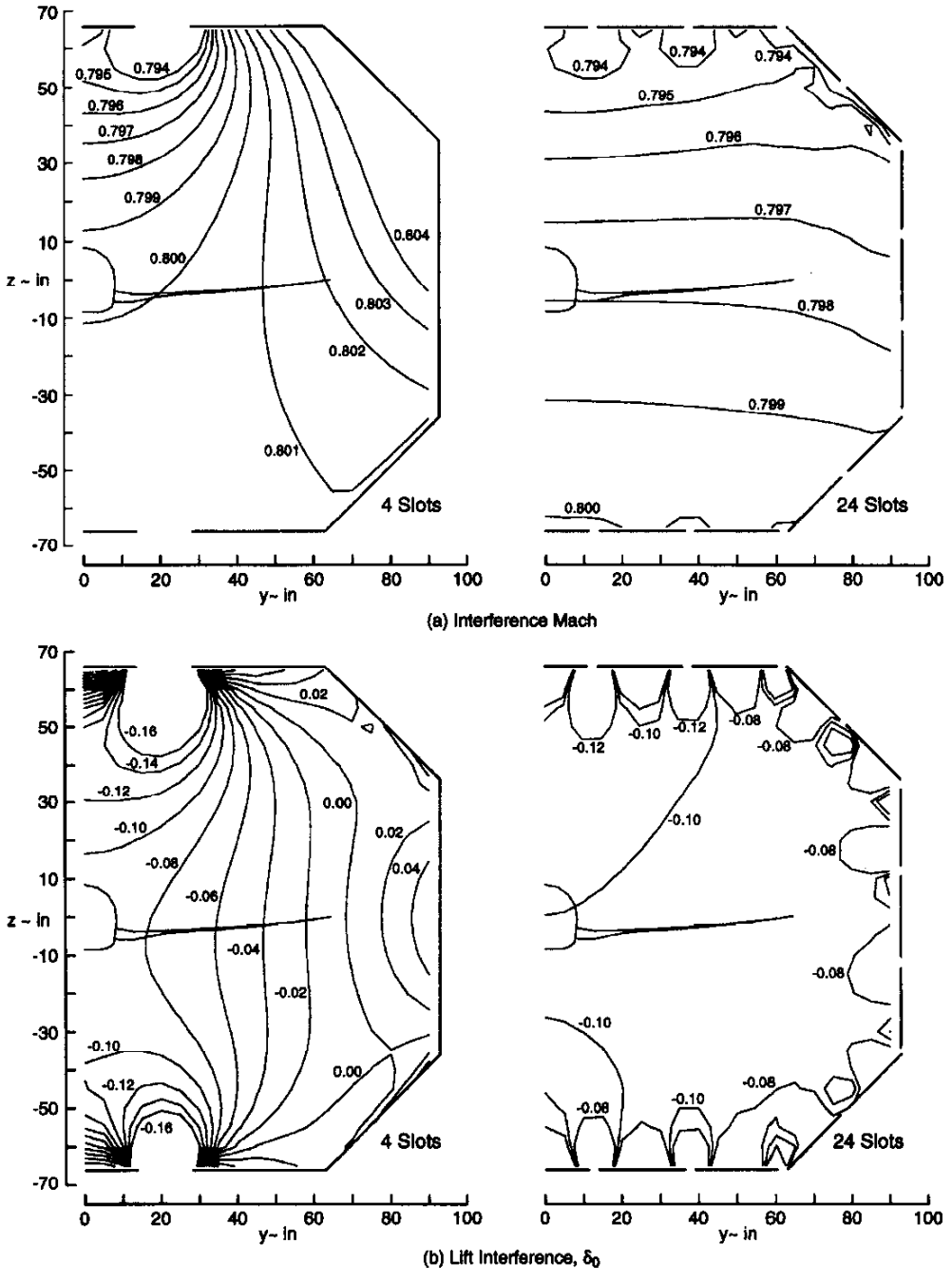

Figure 3.28 : Effect of Number of Slots on Interference in the Vertical Cross-Plane at the Model Centre

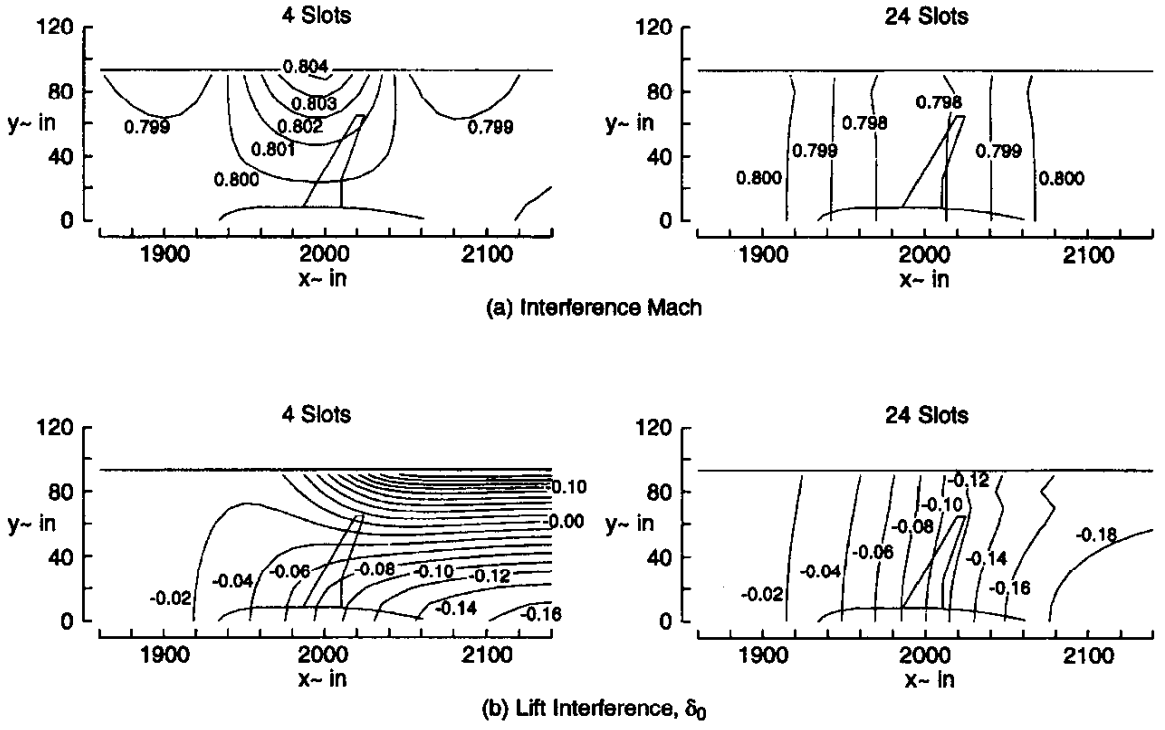

Figure 3.29 : Effect of Number of Slots on Interference in the Horizontal Streamwise Plane through the Model Centre

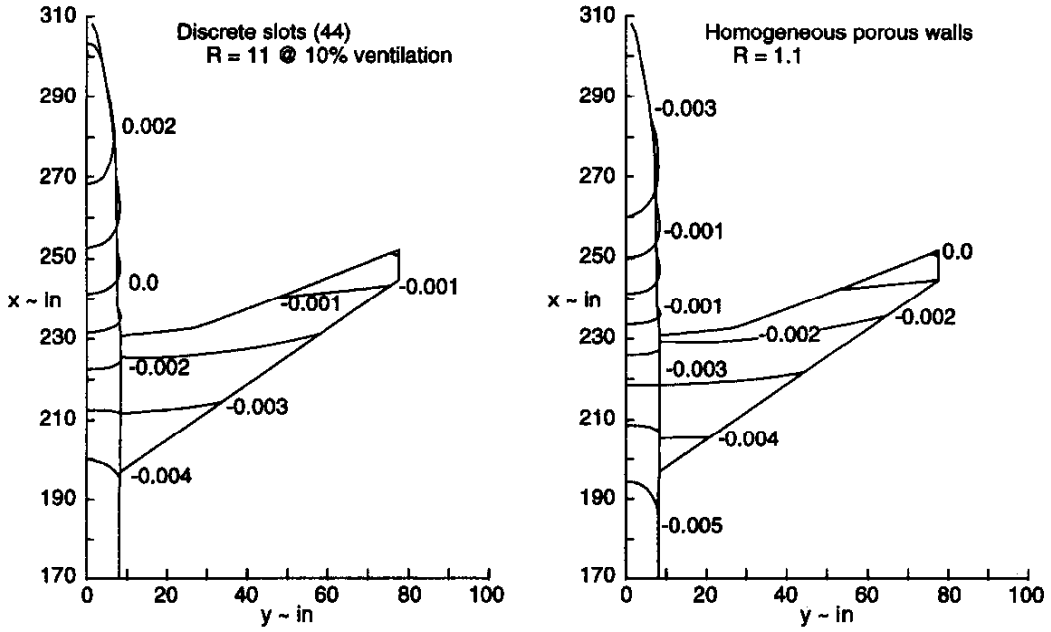

(a) Interference Mach number, ΔM

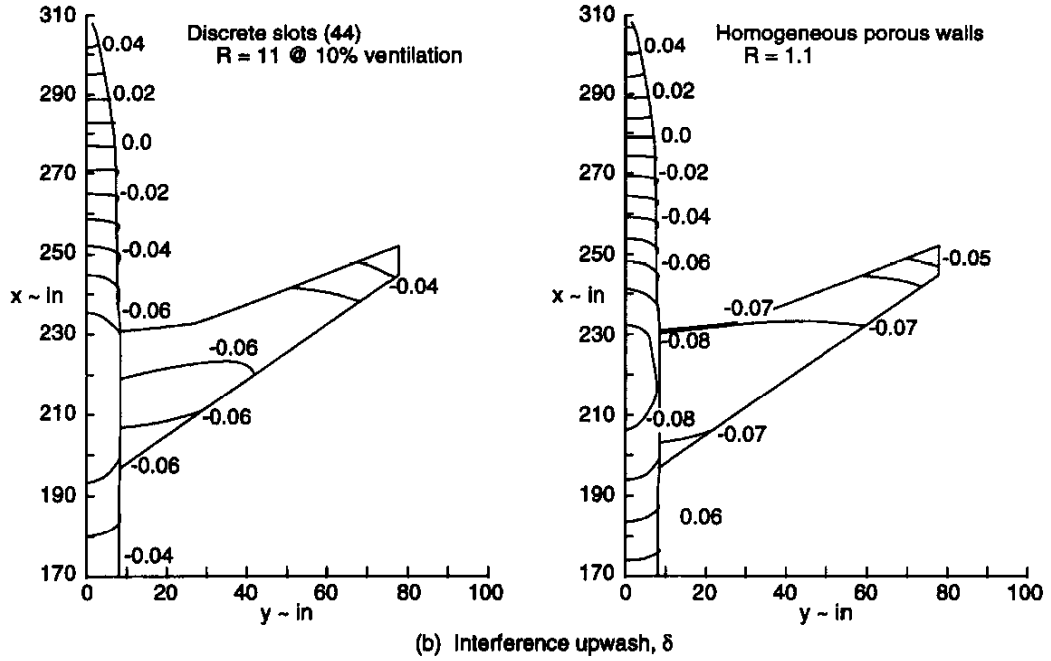

(b) Interference upwash, δ

Figure 3.30 Interference at the Model, Homogeneous Porous Walls and Discrete Slots; M = 0.80, $C_L \cong 0.5$, 2 s/B = 0.83, B/H = 1.41

3.6 CONCLUSION

The validation required of a computational model of a ventilated-wall tunnel depends on required accuracy of the wall correction quantities. Closed-wall and open-jet interference bound interference magnitudes for ideal ventilated walls with uniform characteristics. However, walls that have variable properties or flow fields with significant asymmetry may produce an interference field with strong coupling among the components. Refinement of interference predictions in several large ventilated wind tunnels has led to computational models with modified ideal-wall boundary conditions. These are verified mainly empirically; the deviation of experimental results from ideal wall predictions are usually attributed to non-ideal crossflow characteristics of the walls. Difficulties remain in modelling the downstream portion of a real test section, including the effects of plenum re-entry flow, model support systems, and wall divergence into the test section diffuser. These can especially affect pressure buoyancy forces on the test article. Nevertheless, computational models serve both as a predictive tool and as a stepping stone to boundary measurement methods. Predicted gradients of wall interference, although difficult to validate, are indicators of test situations that may require more sophisticated correction techniques than afforded by linear theory or that may be uncorrectable.

Wall characterisation efforts to date have focused either on direct measurement of wall crossflow characteristics or on correlation of measured pressures "at the wall" with computed pressures. Non-ideal wall behaviour and persistent upward pressure on test model size relative to the test section suggest that customised computational models will continue to be developed for specific ventilated-wall tunnels. As wall validation efforts mature, the decision to shift to boundary measurement methods will depend on a balance of required boundary measurement effort, computational requirements, and the accuracy of alternate methods relative to test objectives.

NOMENCLATURE FOR CHAPTER 3

A	=	effective cross-sectional area of a 2D model
a	=	slot width
B	=	tunnel breadth
b	=	tunnel half-breadth
C	=	cross-sectional area of a test section
C_D	=	drag coefficient
C_L	=	lift coefficient
C_p	=	pressure coefficient
c	=	airfoil chord
D	=	body diameter
d	=	slot spacing
F	=	slotted wall parameter
		$= 2\,K\,/\,H$ for a 2D test section
		$= K\,/\,r_0$ for a circular test section
		$= 2\,K\,/\,H$ for a rectangular test section

H = tunnel height

h = tunnel half-height

K = ideal slot parameter = d / π $\log_e$ (cosec π a / (2d))

L = reference length

M = Mach number

m = source strength = ½ U_X S C_D

P = slotted wall parameter = 1 / (1 + F)

p = static pressure

Q = porous wall parameter = 1 / (1 + β / R)

q = dynamic pressure = ½ ρ U^2

R = porous wall resistance factor

r = cylindrical co-ordinate = $(y^2 + z^2)^{1/2}$

r_0 = radius of circular test section

S = wing reference area

s = wing semi-span

T = blockage shape factor for rectangular tunnels = ε β^3 $(BH)^{3/2}$ / V

t = slot depth (= wall thickness)

t = porous wall parameter = $2/\pi$ arctan(R/β)

U_∞ = upstream reference velocity

u = perturbation velocity in the streamwise (x) direction = $\partial\varphi/\partial x$

V = model effective volume

v = perturbation velocity in the lateral (y) direction = $\partial\varphi/\partial y$

v_{normal} = velocity component normal to the wall

w = perturbation velocity in the vertical (z) direction = $\partial\varphi/\partial z$

x = streamwise spatial co-ordinate

y = spanwise (or lateral) spatial co-ordinate

z = vertical spatial co-ordinate

Greek Symbols

α = angle of attack

β = Prandtl-Glauert compressibility factor = $(1 - M^2)^{1/2}$

δ = lift interference parameter = (w_i / U_X) A / $(S\ C_L)$

δ_0 = lift interference parameter evaluated at model centre

δ_1 = streamwise curvature interference parameter

δ_Ω = upwash interference due to solid blockage

Γs = vortex strength = 1/4 U_∞ S C_L

ε = blockage interference ratio = u_i / U_∞

θ = flow inclination

μ	=	doublet strength = $U_\infty V$
τ	=	tunnel shape factor, or slotted wall openness ratio
Φ	=	total velocity potential
φ	=	perturbation velocity potential
Ω_s	=	streamwise interference parameter due to solid blockage
Ω_w	=	wake blockage interference ratio
Ω_d	=	upwash interference parameter due to solid blockage

Subscripts

i	=	interference
L	=	lower wall
m	=	model
n	=	normal
p	=	plenum (i.e., corresponding to plenum pressure)
S	=	solid (i.e., due to model volume)
U	=	upper wall
W	=	wake (i.e., due to the displacement effect of the model's wake)
w	=	walls

REFERENCES FOR CHAPTER 3

[1] Agrell, N., Pettersson, B., and Sedin, Y. C-J., "Numerical Computations and Measurements of Transonic Flow in a Slotted-Wall Wind Tunnel", AIAA 87-2610, August 1987.

[2] Agrell, N., "Computational Simulations for Some Tests in Transonic Wind Tunnels", paper 14 in AGARD CP-535, October, 1993.

[3] Baldwin, B. S., Turner, J. B., and Knechtel, E. D., *Wall Interference in Wind Tunnels with Slotted and Porous Boundaries at Subsonic Speeds*, NACA TN 3176, May 1954.

[4] Barnwell, R. W., "Improvements in the Slotted-Wall Boundary Condition", Proceedings of the AIAA 9th Aerodynamic Testing Conference, June 1976.

[5] Barnwell, R. W., "Design and Performance Evaluation of Slotted Walls for Two-Dimensional Wind Tunnels", NASA TM 78648, February 1978.

[6] Berndt, S. B., "Inviscid Theory of Wall Interference in Slotted Test Sections", *AIAA Journal*, Vol. 15, September 1977.

[7] Berndt, S. B., "Flow Properties of Slotted-Wall Test Sections", paper 6 in AGARD CP-335, May 1982.

[8] Berndt, S. B. and Sorensen, H., "Flow Properties of Slotted Walls for Transonic Test Sections", paper 17 in AGARD CP-174, October 1975.

[9] Beutner, T. J., Celik, Z. Z., and Roberts, L., "Determination of Solid/Porous Wall Boundary Conditions from Wind Tunnel Data for Computational Fluid Dynamics Codes", paper 16 in AGARD CP-535, July 1994.

[10] Bussoletti, J. E., Huffington, J. R., Krynytzky, A. J., and Saaris, G. R., "CFD Studies in Support of NWTC Test Section Design", AIAA 97-0096, January 1997.

[11] Chan, Y. Y., "Wall Boundary-Layer Effects in Transonic Wind Tunnels", paper 7 in AGARD CP-335, May 1982.

[12] Chen, C. F. and Mears, J. W., "Experimental and Theoretical Study of Mean Boundary Conditions at Perforated and Longitudinally Slotted Wind Tunnel Walls", AEDC TR-57-20, December 1957.

[13] Crites, R. and Rueger, M., "Modelling the Ventilated Wind Tunnel Wall", AIAA 92-0035, January 1992.

[14] Davis, D. D., Jr., and Moore, D., *Analytical Study of Blockage and Lift-Interference Corrections for Slotted Tunnels Obtained by Substitution of an Equivalent Homogeneous Boundary for the Discrete Slots*, NACA RM L53E07b, June 1953.

[15] Engineering Sciences Data Unit, "Lift-interference and blockage corrections for two-dimensional subsonic flow in ventilated and closed wind tunnels.", Item 76028, November 1976; Amend. A, October 1995.

[16] Epton, M. A., "Model Formulation in WALINT", private communication, 1988.

[17] Estabrooks, B. B., "Wall-Interference Effects on Axisymmetric Bodies in Transonic Wind Tunnels with Perforated Wall Test Sections", AEDC TR-59-12, June 1959.

[18] Everhart, J. L., and Barnwell, R. W., "A Parametric Experimental Study of the Interference Effects and the Boundary-Condition Coefficient of Slotted Wind Tunnel Walls", AIAA 78-805, April 1978.

[19] Everhart, J. L., "Theoretical and Experimental Analysis of the Slotted-Wall Flow Field in a Transonic Wind Tunnel", SAE 871757, 1987.

[20] Everhart, J.L., Igoe, W.B. and Flechner, S.G., "Slotted-Wall Flow-Field Measurements in a Transonic Wind Tunnel", NASA TM 4280, August 1991.

[21] Firmin, M. C. P., and Cook, P. H., "Disturbances from Ventilated Tunnel Walls in Aerofoil Testing", RAE Technical Memo AERO 1971, 1983.

[22] Freestone, M. M., and Mohan, S. R., "Interference Determination for Wind Tunnels With Slotted Walls", paper 19 in AGARD-CP-535, July 1994.

[23] Freestone, M. M., Mohan, S. R., and Lock, R.C., „Interference Corrections in Wind Tunnels with Slotted Walls", Paper 16, Proceedings of Conference on „Wind Tunnels and Wind Tunnel Test Techniques", Royal Aeronautical Society, 1992.

[24] Garner, H. C., Rogers, E. W. E., Acum, W. E. A., and Maskell, E. C., "Subsonic Wind Tunnel Wall Corrections", AGARDograph 109, October 1966.

[25] Glauert, H., "Wind Tunnel Interference on Wings, Bodies, and Airscrews", ARC R&M No. 1566, 1933.

[26] Goethert, B. H., *Wind Tunnel Corrections at High Subsonic Speeds Particularly for an Enclosed Circular Tunnel*, NACA TM 1300, 1952.

[27] Goethert, B. H., *Transonic Wind Tunnel Testing*, Pergamon Press, New York, 1961.

[28] Goldhammer, M. E., and Steinle, F. W., Jr., "Design and Validation of Advanced Transonic Wings Using CFD and Very High Reynolds Number Wind Tunnel Testing", 17th ICAS Congress, September 1990.

[29] Holst, H., "German Activities on Wind Tunnel Corrections", paper 4 in AGARD R-692, May 1980.

[30] Holst, H., "Three Dimensional Wall Corrections for Ventilated Wind Tunnels", paper 8 in AGARD CP-335, May 1982.

[31] Holt, D. R. and Hunt, B., "The Use of Panel Methods for the Evaluation of Subsonic Wall Interference", paper 2 in AGARD CP-335, May 1982.

[32] Ivanov, A. I., "An Experimental Study of Gas Flow Near the Perforated Walls of a Transonic Wind Tunnel", *Fluid Mechanics - Soviet Research*, Vol. 17, No. 4, July-August 1988.

[33] Jacocks, J. L., "Determination of Optimum Operating Parameters for the AEDC-PWT 4-Ft Transonic Tunnel with Variable Porosity Test Section Walls", AEDC TR-69-164, August 1969.

[34] Jacocks, J. L., "Aerodynamic Characteristics of Perforated Walls for Transonic Wind Tunnels", AEDC TR-77-61, June 1977.

[35] Johnson, F. T., Samant, S. S., Bieterman, M. B., Melvin, R. G., Young, D. P., Bussoletti, J. E., and Hilmes, C. G., *Tranair: A Full-Potential, Solution-Adaptive, Rectangular Grid Code for Predicting Subsonic, Transonic, and Supersonic Flows About Arbitrary Configurations*, NASA CR 4348, December 1992.

[36] Karlsson, K. R. and Sedin, Y. C-J., "Numerical Design and Analysis of Optimal Slot Shapes for Transonic Test Sections - Axisymmetric Flows", *Journal of Aircraft*, Vol. 18, March 1981.

[37] Keller, J. D., *Numerical Calculation of Boundary-Induced Interference in Slotted or Perforated Wind Tunnels Including Viscous Effects in Slots*, NASA TN D-6871, August 1972.

[38] Keller, J. D., and Wright, R. H., *A Numerical Method of Calculating the Boundary-Induced Interference in Slotted or Perforated Wind Tunnels of Rectangular Cross Section*, NASA TR R-379, November 1971.

[39] Kemp, W. B., Jr., "A Slotted Test Section Numerical Model for Interference Assessment", *Journal of Aircraft*, Vol. 22, March 1985.

[40] Kemp, W. B., Jr., *Computer Simulation of Wind Tunnel Test Section With Discrete Finite-Length Wall Slots*, NASA CR 3948, April 1986.

[41] Kemp, W. B., Jr., *Description and Evaluation of an Interference Assessment Method for a Slotted-Wall Wind Tunnel*, NASA CR 4352, April 1991.

[42] Lee, K. D., "Numerical Simulation of the Wind Tunnel Environment by a Panel Method", AIAA 80-0419, March 1980.

[43] Lo, C. F. and Oliver, R. H., "Boundary Interference in a Rectangular Wind Tunnel with Perforated Walls", AEDC TR-70-67, April 1970.

[44] Matyk, G. E. and Kobayashi, Y., "An Experimental Investigation of Boundary Layer and Crossflow Characteristics of the Ames 2- by 2-Foot and 11- by 11-Foot Transonic Wind-Tunnel Walls", NASA TM 73257, December 1977.

[45] Magnus, A. E. and Epton, M. A., *PAN AIR - Computer Program for Predicting Subsonic or Supersonic Linear Potential Flow About Arbitrary Configurations Using a Higher Order Panel Method, Volume I, Theory Document (Version 1.0)*, NASA CR-3251, 1980.

[46] Mokry, M., " A Wake Blockage Paradox in a Perforated Wall Wind Tunnel", AIAA Journal, Vol. 9, No. 12, Dec 1971.

[47] Mokry, M., Peake, D. J., and Bowker, A. J., "Wall Interference on Two-Dimensional Supercritical Airfoils, Using Wall Pressure Measurements to Determine the Porosity Factors for Tunnel Floor and Ceiling", National Aeronautical Establishment Report LR-575, February 1974.

[48] Mokry, M., and Ohman, L., "Application of the Fast Fourier Transform to Two-Dimensional Wind Tunnel Wall Interference", *Journal of Aircraft*, Vol. 17, June 1980, pp. 402-408.

[49] Mokry, M., "Evaluation of Three-Dimensional Wall Interference Corrections from Boundary Pressure Measurements", National Research Council of Canada LTR-HA-51, November 1980.

[50] Mokry, M., Digney, J. R., and Poole, R. J. D., "Doublet-Panel Method for Half-Model Wind-Tunnel Corrections", *Journal of Aircraft*, Vol. 24, May 1987.

[51] Neiland, V. M., "Optimum Porosity of Wind Tunnel Walls at Low Supersonic Velocities", *Izvestiya Akademii Nauk SSSR, Mekhanika Zhidkosti i Gaza*, No. 4, July-August 1989.

[52] Nyberg, S-E., "Review of Some Investigations on Wind Tunnel Wall Interference Performed in Sweden in Recent Years", paper 6 in AGARD R-692, May 1980.

[53] Pindzola, M., and Lo, C. F., "Boundary Interference at Subsonic Speeds in Wind Tunnels with Ventilated Walls", AEDC TR-69-47, May 1969.

[54] Pounds, G. A., and Walker, J., "Semispan Model Testing in a Variable Porosity Transonic Wind Tunnel", AIAA 80-0461, March 1980.

[55] Schilling, B. L., and Wright, R. H., *Calculated Wind-Tunnel-Boundary Lift-Interference Factors for Rectangular Perforated Test Sections*, NASA TN D-5635, February 1970.

[56] Sedin, Y. C-J., and Sorensen, H., "Computed and Measured Wall Interference in a Slotted Transonic Test Section", *AIAA Journal*, Vol. 24, March 1986.

[57] Sloof, J. W., and Piers, W. J., "The Effect of Finite Test Section Length on Wall Interference in 2-D Ventilated Wind Tunnels", paper 14 in AGARD CP-174, October 1975.

[58] Starr, R. F., "Experiments to Assess the Influence of Changes in the Tunnel Wall Boundary Layer on Transonic Wall Crossflow Characteristics", paper 18 in AGARD CP-174, October 1975.

[59] Steinle, F. W., Jr., and Mabey, "Computer Studies of Hybrid-Slotted Working Sections with Minimum Interference at Subsonic Speeds", NASA TM 86002, August 1984.

[60] Steinle, F. W., Jr., and Pejack, E. R., "Toward an Improved Transonic Wind-Tunnel-Wall Geometry - A Numerical Study", AIAA 80-0442, March 1980.

[61] Steinle, F. W., Jr., and Stanewsky, E., "Wind Tunnel Flow Quality and Data Accuracy Requirements", AGARD AR-184, November 1982.

[62] Theodorsen, T., *The Theory of Wind Tunnel Wall Interference*, NACA Report 410, 1931.

[63] Vaucheret, X., "Reduction des corrections de parois en veines d'essais transsoniques classiques a l'aide d'etudes parametriques sur ordinateur", ONERA TP 1976-60, June 1976.

[64] Vaucheret, X. and Vayssaire, J, C., "Corrections de parois en ecoulement tridimensionnel transsonique dans des veines a parois ventilees", paper 16 in AGARD CP-174, October 1975.

[65] Vaucheret, X., "Ameliorations des calculs des effets de parois dans les souffleries industrielles de l'ONERA", paper 11 in AGARD-CP-335, May 1982.

[66] Vaucheret, X., "Vortex Lattice Code for Computation of Wind Tunnel and Support Effects on Models", *La Recherche Aerospatiale* (English edition), No. 1991-2, pp. 39-51.

[67] Vayssaire, J. C., "Survey of Methods for Correcting Wall Constraints in Transonic Wind Tunnels", AGARD R-601, April 1973.

[68] Wu, J. M., Collins, F. G., and Bhat, M. K., "Three-Dimensional Flow Studies on a Slotted Transonic Wind Tunnel Wall", AIAA 82-0230, January 1982.